Metastable Phase Separation and Information Retrieval in Multicomponent Liquids

Davide Marcato[*]
Gulbenkian Institute of Molecular Medicine, 2780-156 Oeiras, Portugal

Rodrigo Braz Teixeira[*]
Gulbenkian Institute of Molecular Medicine, 2780-156 Oeiras, Portugal and Centro de Física Teórica e Computacional, Faculdade de Ciências, Universidade de Lisboa, 1749-016 Lisboa, Portugal

Izaak Neri[‡]
Department of Mathematics, King's College London, Strand, London, WC2R 2LS, United Kingdom

Pablo Sartori[†]
Gulbenkian Institute of Molecular Medicine, 2780-156 Oeiras, Portugal

(Received 26 September 2025; revised 25 June 2026; accepted 20 August 2026; published 5 November 2026)

Liquid mixtures can separate into phases with distinct composition. This phenomenon has recently come back to prominence due to its role in complex biological liquids, such as the cytoplasm, which contain thousands of components. For simple two-component mixtures phase-separated states are global free energy minima. However, local free energy minima, i.e., metastable states, are known to play a dominant role in complex systems with many components. For example, Hopfield neural networks can retrieve stored information from partial cues via relaxation to metastable states. Under what conditions can phase separated states be metastable, and what are the implications for information retrieval in multicomponent liquids? In this work we develop the general thermodynamic formalism of metastable phase separation. We then apply this formalism to an illustrative toy example inspired by recent experiments, binary mixtures with high-order interactions. Finally, as core application of the formalism, we study metastability in Hopfield liquids, a class of multicomponent mixtures capable of storing information on the composition of phases. We show that these phases can be nucleated from partial cues via metastable phase separation. Spatial simulations of liquids with a large number of components match our analytical solution. Our work suggests that complex biological mixtures can retrieve information through metastable phase separation.

DOI: 10.1103/lxrw-98f4

Subject Areas: Biological Physics, Soft Matter, Statistical Physics

I. INTRODUCTION

Phase separation is the phenomenon by which a mixture of multiple components spatially segregates into regions with different composition. Common intuition on phase separation derives from results for binary mixtures [1–3]. Yet, some of the liquids most studied today, such as the cellular cytoplasm, nucleoplasm, and plasma membrane, consist of thousands of different components [4]. These liquids segregate into phases of distinct composition, called biomolecular condensates [5], that coexist with each other. For example, in the nucleoplasm a dozen condensates, including Cajal bodies, paraspeckles, and nucleoli, have been identified [6,7]. These condensates can be composed of hundreds of distinct macromolecular components [8,9], and several of these components are shared among different condensates [10]. Given that a mixture with $N \gg 1$ components allows for a vast number of possible phases, it is remarkable that biological liquids reliably separate into phases with specific compositions [11–15]. Because of the high complexity of this problem, a general theoretical framework capable of predicting the emergent phase separated states of a mixture with many components is lacking.

The thermodynamics of a liquid mixture can be characterized by a free energy functional, which for $N \gg 1$ is defined on a high-dimensional space [16]. At high temperature this functional has a single global minimum, the

[*]These authors contributed equally to this work.
[†]Contact author: pablo.sartori@gimm.pt
[‡]Contact author: izaak.neri@kcl.ac.uk

Published by the American Physical Society under the terms of the Creative Commons Attribution 4.0 International license. Further distribution of this work must maintain attribution to the author(s) and the published article's title, journal citation, and DOI.

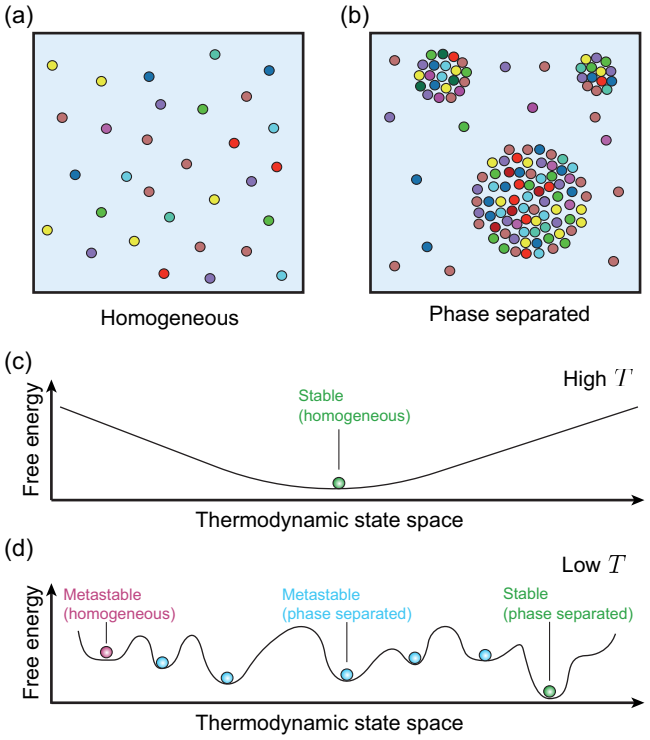


FIG. 1. Metastable states in multicomponent mixtures. (a) Schematic of a homogeneous state in a multicomponent mixture (solutes represented by colored circles, solvent by blue background). (b) Schematic of a phase separated state in a multicomponent mixture. Several droplets of diverse sizes and compositions can coexist in such states. (c) Representation of the free energy landscape for a mixture with many components at fixed state parameters. At high temperature, there is only one stable state, which is the homogeneous state. (d) Same as (c), but at lower temperatures. In this case, the homogeneous state is only one of many possible metastable states. All other metastable states are phase separated, including the global minimum corresponding with the thermodynamic equilibrium.

homogeneous phase, which is a state of thermodynamic equilibrium [Figs. 1(a) and 1(c)]. In contrast, at low temperature the free energy functional can have multiple metastable states, as functions in high dimensions can have many minima. These states are stable towards small thermal fluctuations and can be long lived. Metastability in liquids is commonly associated with homogeneous states, because for simple binary mixtures the homogeneous states are metastable between the binodal and spinodal lines [1–3]. However, generically, phase separated states can also be metastable, and therefore at low temperature mixtures with $N \gg 1$ can exhibit many metastable phase separated states [Figs. 1(b) and 1(d)].

Besides the above general argument, there are multiple reasons why metastability is expected to play a central role in the physics of multicomponent mixtures. We highlight two. First, metastable states are abundant in complex systems with a large number of components and/or heterogeneous interactions, such as proteins [17,18], spin glasses [19,20], granular materials [21], or Hopfield neural networks [22], and recent work shows that metastable states are also abundant in multicomponent mixtures [11,23]. Second, it has been experimentally observed that some biological liquid mixtures phase separate at short times, yet transition to a different equilibrium phase at longer times [24–27]. Therefore, based on analogy with other complex systems and recent experiments, we expect metastability to be a crucial ingredient of phase separation in multicomponent mixtures.

In this paper, we develop the general thermodynamic formalism of metastable phase separation in multicomponent mixtures. We derive the conditions for stationarity and metastability of phase separated states in multicomponent mixtures. We then discuss two applications. First, we develop a simple model for metastable phase separation in binary mixtures, and we show that this model exhibits the same metastable phase separation phenomenology as observed in experiments with prionlike proteins [24–27]. As a second application of metastable phase separation, we develop a liquid version of an associative memory, previously named the liquid Hopfield model [11,28], that can demix into metastable phases that are enriched and depleted in a prescribed set of components. Note that this is different from the analysis of the liquid Hopfield model in Ref. [11], which did not involve phase separation but retrieval of homogeneous states. As we show, these target phases can be retrieved through the nucleation of seeds that are enriched in some but not all the prescribed components, even though the system has a large number of metastable states. This mechanism of controlled phase separation is similar to memory retrieval in the Hopfield model [22,29–31]. It implies that the number of metastable nontarget states is small enough so that the system does not exhibit a glassy dynamics.

The paper is structured as follows. In Secs. II to IV we develop the thermodynamic formalism of metastable phase separation. Section V analyzes a simple but illustrative example, binary mixtures with higher-order interactions. Section VI investigates the retrieval of phases of prescribed compositions through nucleation in Hopfield liquids, which are a liquid analog of associative memory. Finally, Sec. VII discusses our results in the context of existing literature.

II. THERMODYNAMICS OF MULTICOMPONENT MIXTURES

We start by presenting the thermodynamics of an incompressible multicomponent liquid mixture. We focus on the canonical ensemble in which the system of interest is contained in a rigid vessel, in contact with a thermal reservoir, and prevented from any material exchanges with the outside (see Supplemental Material [32] Sec. S1 for an equivalent analysis in the grand canonical ensemble). We discuss two sets of states for the mixture: spatially

homogeneous states and spatially heterogeneous states. We call the latter phase separated states. In the present section, these states are discussed without reference to their stationarity or stability, as stationarity and stability will be addressed in subsequent sections.

A. Spatially homogeneous states

Consider a spatially homogeneous multicomponent mixture of N distinct solute components, labeled by $i = 1, \ldots, N$, that are dissolved in a solvent component, labeled by $i = 0$. The mixture is in contact with a thermal reservoir at temperature T, and is confined within a rigid vessel of volume V. The vessel is closed, and we assume that no chemical reactions occur: therefore, the number of molecules of the solvent, M_0, and of the N solute components, $\vec{M} = (M_1, \ldots, M_N)$, are fixed. We additionally assume that the solvent and solutes are all incompressible, which implies that the number of molecules of one of the species, which we take to be M_0, is not needed to specify the state of the system, see Appendix A. Thus, the $N + 2$ thermodynamic state parameters are $\vec{M}$, T, and V.

The thermodynamics of this system is described by the Helmholtz free energy [16,38].

$$F = F(T, V, \vec{M}), \tag{1}$$

The free energy density, $f = F/V$, depends only on $N + 1$ variables

$$f = f(T, \vec{\phi}), \tag{2}$$

where we have defined the volume fractions of the solute components as $\phi_i = \nu_i M_i / V$, with ν_i the molecular volumes. As we focus on the incompressible case, the ν_i are constant (i.e., independent of T, V, and $\vec{M}$), see Appendix A. The volume fraction of the solvent is given by $\phi_0 = 1 - \sum_{i=1}^{N} \phi_i$. Therefore, the parameters $\vec{\phi}$ are subject to the constraint $\sum_{i=1}^{N} \phi_i \leq 1$. In what follows, we will refer to $\vec{\phi}$ as the composition vector, unless otherwise specified.

The dependent intensive thermodynamic quantities can be computed in terms of partial derivatives of $f(T, \vec{\phi})$. For example, the exchange chemical potentials of the solutes are

$$\bar{\mu}_i = \nu_i \left(\frac{\partial f}{\partial \phi_i} \right)_{T, \vec{\phi}'}, \tag{3}$$

where $'$ denotes that the vector excludes component i; and the osmotic pressure is

$$\Pi = -f + \vec{\mu} \cdot \vec{\rho}, \tag{4}$$

where we have introduced the number densities of the solutes, $\rho_i = \phi_i / \nu_i$. In (4), $\vec{\mu} = \vec{\bar{\mu}}$ is the vector of exchange potentials. The usage of osmotic pressure and exchange chemical potential arises from incompressibility. In the case of chemical potentials, a change in the abundance of a solute must be compensated by a change in the abundance of a solvent, so the total volume does not change. Analogously, the change in volume required to compute the pressure is associated with adding or removing solvent molecules.

In Secs. III–IV, which develop the general formalism of phase separation, we will not consider any specific form of the free energy of homogeneous states. In later sections, we will consider specific functional forms of $f(T, \vec{\phi})$ that correspond to the continuous limit of a lattice gas [1]. These are best described by separating the free energy density into energetic and entropic contributions, i.e., $f = u - Ts$. Without loss of generality, we take for the energy density a function of the form

$$u(\vec{\phi}) = -\frac{v_2}{2\nu_0} \sum_{ij} J_{ij} \phi_i \phi_j + \frac{v_3}{6\nu_0} \sum_{ijk} K_{ijk} \phi_i \phi_j \phi_k + \ldots, \tag{5}$$

where the affinity matrix J_{ij} determines the pairwise interactions, the tensor K_{ijk} determines the three-body interactions, etc. The strength of the interactions is determined by v_2, v_3, etc., which have units of energy. The entropy density is taken to be

$$s(\vec{\phi}) = -\frac{k_B}{\nu_0} \sum_{i=1}^{N} \phi_i \log(\phi_i) - \frac{k_B}{\nu_0} \phi_0 \log(\phi_0), \tag{6}$$

where k_B is Boltzmann's constant and the second term corresponds to the entropic contribution of the solvent. In this expression we have used the simplifying assumption that the molecular volumes of all solutes are equal to that of the solvent, i.e., $\nu_i = \nu_0$. In what follows we will measure energy in units of $k_B T$. We do not set $\nu_0 = 1$, as later we shall consider a spatially resolved model.

B. Phase separated states

We now describe the thermodynamics of multicomponent mixtures in phase separated states. Such states can be described through multiple compartments, labeled by $c = 1, \ldots, C$, each representing a homogeneous state of the mixture. Each compartment is characterized by a composition vector, $\vec{\phi}^{(c)}$, and the volume of the compartment, $V^{(c)}$. Note that multiple compartments can share the same composition vector. As will become clear later, this redundancy is necessary because the number of different phases is not known *a priori*.

We associate to phase separated states the free energy functional $\mathfrak{F} = \sum_{c=1}^{C} V^{(c)} f(T, \vec{\phi}^{(c)})$. Here, "fraktur" fonts are used for spatially heterogeneous free energies. Defining the intensive free energy functional as $\mathfrak{f} = \mathfrak{F}/V$, we obtain

$$\mathfrak{f}(T,\{w^{(c)}\},\{\vec{\phi}^{(c)}\}) = \sum_{c=1}^{C} w^{(c)} f(T,\vec{\phi}^{(c)}), \tag{7}$$

where we have defined the volume fractions of the compartments as $w^{(c)} = V^{(c)}/V$. For simplicity, we refer in what follows to the $w^{(c)}$ as the compartment volumes. Above, and in what follows, we use curly brackets to denote vectors for which the entries are associated with the compartments. Furthermore, with slight abuse of notation, we will use the superindex $^{(c)}$ to denote functions evaluated at $\vec{\phi}^{(c)}$, e.g., $f^{(c)} = f(T,\vec{\phi}^{(c)})$. Notice that the functional (7) does not include a contribution due to surface tension. In Secs. V and VI we will include surface tension into the model, as we will consider the effect of space on phase separation.

As we are working in the canonical ensemble with parameters $(T, V, \vec{M})$, the variables $w^{(c)}$ satisfy the volume constraint

$$\sum_{c=1}^{C} w^{(c)} = 1, \tag{8}$$

which we will often use to express the volume of compartment C as $w^{(C)} = 1 - \sum_{c<C} w^{(c)}$. The variables $\{\vec{\phi}^{(c)}\}$ satisfy the constraints

$$\sum_{c=1}^{C} w^{(c)} \phi_i^{(c)} = \phi_i. \tag{9}$$

As the variables, $\{w^{(c)},\vec{\phi}^{(c)}\}$, span an $(N+1)C$ dimensional space, and Eqs. (8) and (9) constitute $N+1$ constraints, the allowed subspace for the variables has $(C-1)(N+1)$ dimensions.

The thermodynamic equilibrium state of the liquid mixture is obtained by minimizing the functional $\mathfrak{f}$ with respect to its variables $\{w^{(c)}\}$, $\{\vec{\phi}^{(c)}\}$ and C, subject to the constraints in Eqs. (8) and (9). The minima of $\mathfrak{f}$ represent the equilibrium state, which is a function of the external parameters. The number of phases P in the equilibrium configuration equals the number of compartments with different compositions. Notice that there exist redundant representations of the equilibrium configurations for which $C > P$, and thus $\mathfrak{f}$ has multiple minima representing the equilibrium configuration. As already mentioned, since *a priori* the number of phases P in the equilibrium state is not known, it is necessary to allow for this redundancy.

III. STATIONARITY CONDITIONS

As anticipated in the Introduction, metastable states are expected to play an important role in the physics of phase separation in multicomponent mixtures. To initiate the study of metastable states, we derive in this section conditions for stationarity in multicomponent mixtures. Note that a stationary state can be either a minimum, maximum, or saddle point of the free energy functional.

Phase separated states are stationary if conditions of chemical and mechanical balance are satisfied. Chemical balance implies that the exchange chemical potentials of any given species i are the same across all compartments, i.e.,

$$\bar{\mu}_i^{(c)} = \bar{\mu}_i^{(c')} \tag{10}$$

for all pairs of compartments c and c'. Mechanical balance implies that the osmotic pressures of all compartments are identical, and so

$$\Pi^{(c)} = \Pi^{(c')} \tag{11}$$

for all pairs of compartments c and c'.

We remark that the above conditions are necessary conditions for minimizing the free energy in Eq. (7), but they are not sufficient. This crucial distinction is sometimes overlooked in the literature [39,40], where it is stated that when Eqs. (10) and (11) are satisfied the free energy is minimized. However, it is entirely possible that Eqs. (10) and (11) are satisfied in a maximum or a saddle of the free energy. To guarantee that a stationary point is a minimum additional conditions must be tested, as we discuss later.

To derive the above conditions, we determine how the free energy $\mathfrak{f}$ changes in response to a small arbitrary perturbation that complies with the constraints of the system. In particular, consider a state $(\{w^{(c)}\},\{\vec{\phi}^{(c)}\})$, and a perturbed state near it with compartment volumes $\tilde{w}^{(c)} = w^{(c)} + \epsilon^{(c)}$ and compositions $\tilde{\phi}_i^{(c)} = \phi_i^{(c)} + \delta_i^{(c)}$, where $|\epsilon^{(c)}| \ll 1$ and $|\delta_i^{(c)}| \ll 1$ are perturbation parameters. The perturbation must comply with the constraints in Eqs. (8) and (9), which render $\delta_i^{(C)}$ and $\epsilon^{(C)}$ perturbation dependent functions, see Appendix B for explicit expressions. Then, we evaluate the change in free energy, $\Delta\mathfrak{f} = \tilde{\mathfrak{f}} - \mathfrak{f}$, to linear order in the perturbation, where $\tilde{\mathfrak{f}}$ is the free energy of the perturbed state. The stationarity conditions are obtained by setting all linear terms in the expression of $\Delta\mathfrak{f}$ to zero, see Appendix C. Setting to zero the terms in $\delta_i^{(c)}$ returns the chemical balance conditions (10), and setting to zero the terms in $\epsilon^{(c)}$ returns the mechanical balance conditions (11). In conclusion, the stationary states of the liquid mixture are found by solving Eqs. (10) and (11) together with the constraints (8) and (9). Notice that a homogeneous state is characterized by the same composition in each compartment: hence, the chemical and mechanical balance conditions are always satisfied, and all homogeneous states are stationary (see Supplemental Material Sec. S2 [32] for a more detailed discussion).

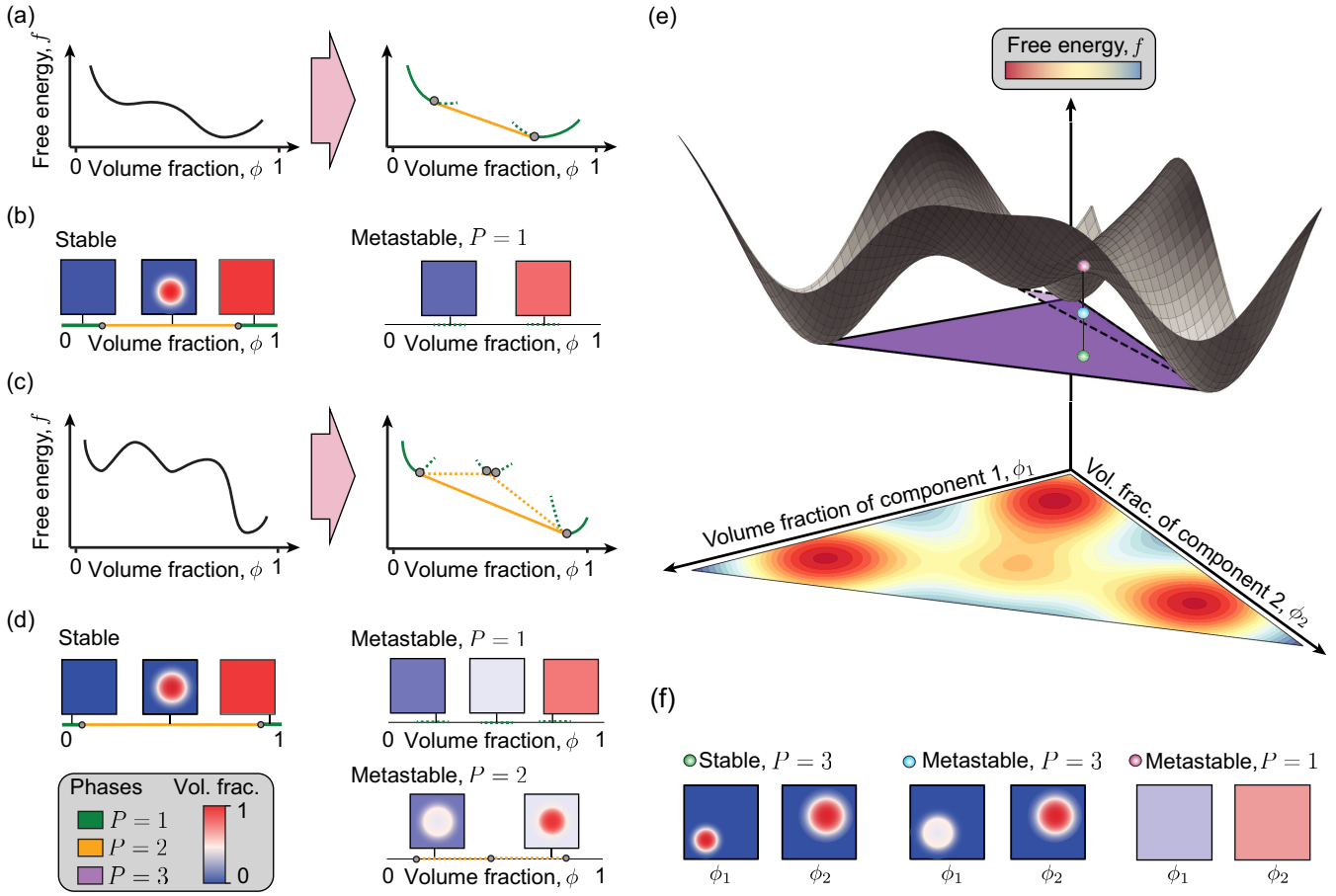


FIG. 2. Schematic illustration of the geometry underlying metastable phase separation. (a) Standard binary mixtures admit a single phase separated state, which can be found by the common tangent construction (orange line connecting two gray circles). The only metastable states are homogeneous states (dashed green line) (b) The geometry of the state space of a binary mixture is a straight line. The phase separated state is stable at intermediate solute volume fractions, with high and low volume fractions corresponding to stable homogeneous phases. In addition, there are two metastable regions corresponding to homogeneous phases. The square images show schematics of 2D spatial simulations of the system. (c) In presence of nonlinear interactions, binary mixtures may admit multiple phase separated states, corresponding to multiple common tangent constructions (three in this example, corresponding to the orange solid line and the two orange dashed lines). (d) Besides globally stable phase separated states and homogeneous metastable states, the system in (c) also admits two metastable phase separated states. Gray box contains color legend. (e) For a ternary mixture the state space geometry is a triangle. Because of the increase in dimensionality the system now admits a large variety of common tangent lines and planes (three examples are shown, corresponding to the violet planes and the red point). Of these, only those belonging to the convex hull correspond to stable equilibrium states. (f) Examples of a stable phase separated state, a metastable phase separated state, and a metastable homogeneous state. The three states correspond to the same thermodynamic parameters, as can be seen by the corresponding points (green, blue, red) that appear in panel (e). This figure is analogous to Fig. 1(d). However, now we have two species, $N = 2$, and thus we need to specify the spatial distribution of both ϕ_1 and ϕ_2.

Equations (10) and (11) have a useful geometrical interpretation: solving them is equivalent to finding a set of points of the free energy surface that share a common tangent hyperplane (see Appendix C). Different tangent hyperplanes correspond to different stationary states, see Fig. 2.

Finally, notice how the fact that Eqs. (10) and (11) depend only on the composition vectors $\{\vec{\phi}^{(c)}\}$ ultimately imposes an upper bound to the possible values of P. As we count $(N+1)(P-1)$ equations and PN variables, and as the number of equations should be smaller or equal than the number of variables in order to avoid an overconstrained system, we conclude that

$$P \leq N + 1, \tag{12}$$

which is the celebrated Gibbs phase rule [3,38].

IV. STABILITY CONDITIONS

We next derive stability conditions for stationary states. These determine whether a particular stationary state is a

maximum, saddle, or minimum. We are particularly interested in minima, of which there are two kinds: local minima, which represent metastable states; and global minima, which represent thermodynamic equilibrium states. Although metastability is commonly associated with homogeneous states, phase-separated states may also be metastable, see Refs. [41–44] for examples. Also, as briefly mentioned in the Introduction, metastable liquid droplets have been observed in *in vitro* experiments involving prionlike proteins or peptides at physiological concentrations [24–27]. Here we derive the conditions for the metastability of phase separated states in multicomponent mixtures.

The key result of this section is a proof of the following statement: a phase separated state with P phases is metastable if and only if the Hessians $\mathbf{h}^{(c)} = \mathbf{h}(\vec{\phi}^{(c)})$ for each of the compartments corresponding to different phases are positive definite. Hence, metastability of a phase separated state is equivalent (necessary and sufficient) to metastability of the phases it is composed of. Note that for phase separated states there are two kinds of perturbations that respect the constraints of the canonical ensemble: those that change the volumes and compositions of the existing phases, and those that nucleate new phases.

We first show that if the Hessians $\mathbf{h}^{(c)}$ are all positive definite, then the free energy of the mixture cannot decrease by implementing one of these perturbations. This demonstrates that metastability of all phases is sufficient for metastability of the phase separated state. To this purpose, we analyze the convexity of the free energy, $\mathfrak{f}$, in terms of its variables $\{w^{(c)}\}$ and $\{\vec{\phi}^{(c)}\}$. As in the case of stationarity, this convexity analysis is subject to the constraints in Eqs. (8) and (9). We therefore compute the free energy difference $\Delta\mathfrak{f}$ to second order in the perturbation (see Appendix B). Due to stationarity the linear terms vanish, and the remaining quadratic term can be written as (see Appendix D)

$$\Delta\mathfrak{f}(\{\vec{\delta}^{(c)}\}', \{\epsilon^{(c)}\}') = \frac{1}{2}\sum_{c=1}^{C} w^{(c)} \sum_{i,j=1}^{N} \delta_i^{(c)} \delta_j^{(c)} h_{ij}^{(c)}, \quad (13)$$

where the prime indicates that there is no explicit dependence on the Cth volume or composition perturbations. This latter fact is due to the constraints in Eqs. (8) and (9), which allows us to write

$$\delta_i^{(C)} = -\sum_{c=1}^{C-1} \delta_i^{(c)} \frac{w^{(c)}}{w^{(C)}} + \sum_{c=1}^{C-1} \epsilon^{(c)} \frac{(\phi_i^{(C)} - \phi_i^{(c)})}{w^{(C)}}, \quad (14)$$

and $\epsilon^{(C)} = -\sum_{c=1}^{C-1} \epsilon^{(c)}$. From Eq. (13) it follows that, in general, $\Delta\mathfrak{f}$ is positive if all the Hessians $\mathbf{h}^{(c)}$ are positive definite.

Note that Eq. (13) does not rule out the possibility of *soft modes*. These are perturbations that alter the volume fractions without altering the composition of the phases, so that $\delta_i^{(c)} = 0$ for every i and every c, while some of the $\epsilon^{(c)} \neq 0$. These soft modes leave the free energy unaltered, $\Delta\mathfrak{f} = 0$, even if the Hessians are positive definite, and for such liquid mixtures the stable state is degenerate. Such soft modes occur in the liquid Hopfield model of Sec. VI.

We next show that if one phase has a Hessian with negative eigenvalues, then there will always be a perturbation that decreases the free energy. This demonstrates that metastability of all phases is not just sufficient, but also necessary for metastability of the phase separated state. A naive look at Eq. (13) may suggest that a state can be metastable, even if one phase is unstable, viz., because the Hessians of the other phases have positive eigenvalues. However, this argument does not consider perturbations that nucleate a new phase. If one phase has a negative eigenvalue, then the free energy of the liquid mixture can be reduced by nucleating a new phase inside the unstable phase, a type of instability that requires using $C > P$. This instability is similar to that of homogeneous states when it crosses the spinodal boundary, but here it applies for phase separated states (see Appendix D for details).

Metastable states in multicomponent mixtures have a simple geometric interpretation, as illustrated in Fig. 2. Indeed, metastable states represent simplexes located on affine subspaces that are tangent to the free energy function $f(\vec{\phi})$. The dimension of the tangent affine subspace equals the number of phases that compose the spatially heterogeneous state minus one. For example, a heterogeneous state of three phases is represented by a triangle on a plane tangent to $f(\vec{\phi})$, as illustrated in Fig. 2 (see also Appendix C).

V. METASTABLE PHASE SEPARATION IN BINARY MIXTURES

We revisit metastable phase separation in binary mixtures consisting of a solvent and a single solute [42,43], as a simple introductory example, before turning to metastable phase separation in multicomponent mixtures in the following section. We begin by applying the formalism developed in Secs. II–IV to identify the metastable states. This analytical approach is then validated using continuum-space simulations that incorporate both diffusion and surface tension.

A. Theoretical results

We consider a mixture with one solute component, $N = 1$, that can phase separate from the solvent. The free energy takes the form

$$f(\phi) = u(\phi) + \frac{1}{\nu_0}\phi\log\phi + \frac{1}{\nu_0}(1-\phi)\log(1-\phi), \quad (15)$$

where $\phi = \phi_1$ is the composition vector, here a scalar, and we removed the subindex 1 [2]. In this section we will refer to ϕ as the solute volume fraction. This model can be found in textbooks for the case in which $u(\phi)$ is quadratic [1,2], of which the Flory-Huggins model is a particular example [45] (see Supplemental Material Sec. S4 [32]). Here we will show that phase separated metastable states can arise when $u(\phi)$ has a higher order nonlinearity, as illustrated in Figs. 2(c) and 2(d) (see also Supplemental Material Sec. S5 [32] for mathematical details). As an example we consider

$$u(\phi) = -\frac{c}{12\nu_0}\left(\phi - \frac{1}{2}\right)^4, \tag{16}$$

where the constant c, which has units of energy, quantifies the strength of the interaction.

Figures 3(a) and 3(b) display representative plots of $f(\phi)$ for two different values of c. Metastable homogeneous states are obtained by identifying convex regions in the graph $f(\phi)$ (represented by dashed lines). Metastable phase separated states are obtained from constructing tangent lines to the graph $f(\phi)$ that connect two points in which the function is convex. Unlike in the case of binary mixtures with a quadratic energy function, this graph allows for three different tangent constructions, given by the straight lines in Figs. 3(a) and 3(b), corresponding with three families of phase separated states. One line connects low and high volume fractions (family I, in red), another connects low and intermediate volume fractions (family II, in green), and another connects intermediate and high volume fractions (family III, in blue). Depending on the value of the interaction parameter c and the thermodynamic control parameter ϕ, the globally stable state will be either a homogeneous state or a phase separated state from one of the families. For example, at $c = 120$ and $\phi = 0.25$, the equilibrium state is a phase separated state from family II, while phase separated states from family I are metastable. On the other hand, for $c = 135$ and $\phi = 0.25$, the equilibrium state is a member of family I, and family II is metastable.

Panel (c) of Fig. 3 shows lines delimiting the regions where the different phases are stable. The spinodal line of the homogeneous phase (solid pink line) separates the region of low c for which the homogeneous state is metastable from the region at high c where it is unstable. The spinodal of the homogeneous phase is obtained from solving the equation $f''(\phi_{sp}) = 0$ towards ϕ_{sp}, which admits an analytical solution (see Supplemental Material Sec. S5 [32]). The regions that are enclosed by the other three solid lines denote the regions for which the phase separated states are stable (red, green, and blue solid lines, and the corresponding shaded regions, refer to the three families). These lines are obtained by finding all solutions

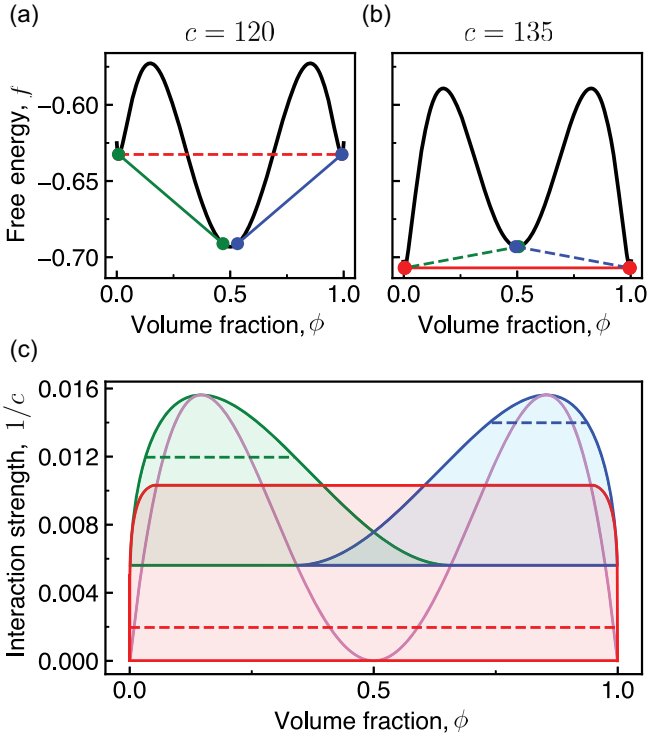


FIG. 3. Free energy and stability diagram for a binary mixture with quartic potential. (a) Free energy density $f(\phi)$, in units of ν_0^{-1}, from Eq. (15) with the energy function in Eq. (16) for $c = 120$. Common tangent lines correspond to phase separated states, solid lines are stable and dashed metastable (see Supplemental Material Sec. S5 [32] for more details). (b) Same as in (a), but for $c = 135$. Stability is reversed: metastable states in (a) become stable, and the stable state in (a) is now metastable. (c) Stability diagram in the (c^{-1}, ϕ) parameter space, with c^{-1} the inverse interaction energy and ϕ the volume fraction of the solute. The spinodal line of the homogeneous state is plotted in pink. There are three additional lines delineating the regions where the three phase separated states are stable: high and low volume fraction (red, family I), low and intermediate volume fraction (green, family II), and high and intermediate volume fraction (blue, family III). The corresponding binodal lines can be found in Supplemental Material Fig. S3 [32]. Tie lines are given by horizontal lines connecting coexisting volume fractions in the phase separated states, three examples are shown: one for $c = 71$ (blue dashed line), one for $c = 83$ (green dashed line) and another for $c = 500$ (red dashed line). A phase diagram can be constructed by selecting the phase of lowest free energy for each parameter, see Supplemental Material Fig. S3 [32].

to the common tangent conditions for different values of c. The three dashed lines correspond to three tie lines that connect the volume fractions of the two phases that compose phase separated states of each family (see Supplemental Material Sec. S5 [32] for explicit expressions). Observe that at intermediate values of c multiple states are metastable. In these regions the thermodynamic equilibrium state is found by comparing the free energies of the different metastable states (see Fig. 3).

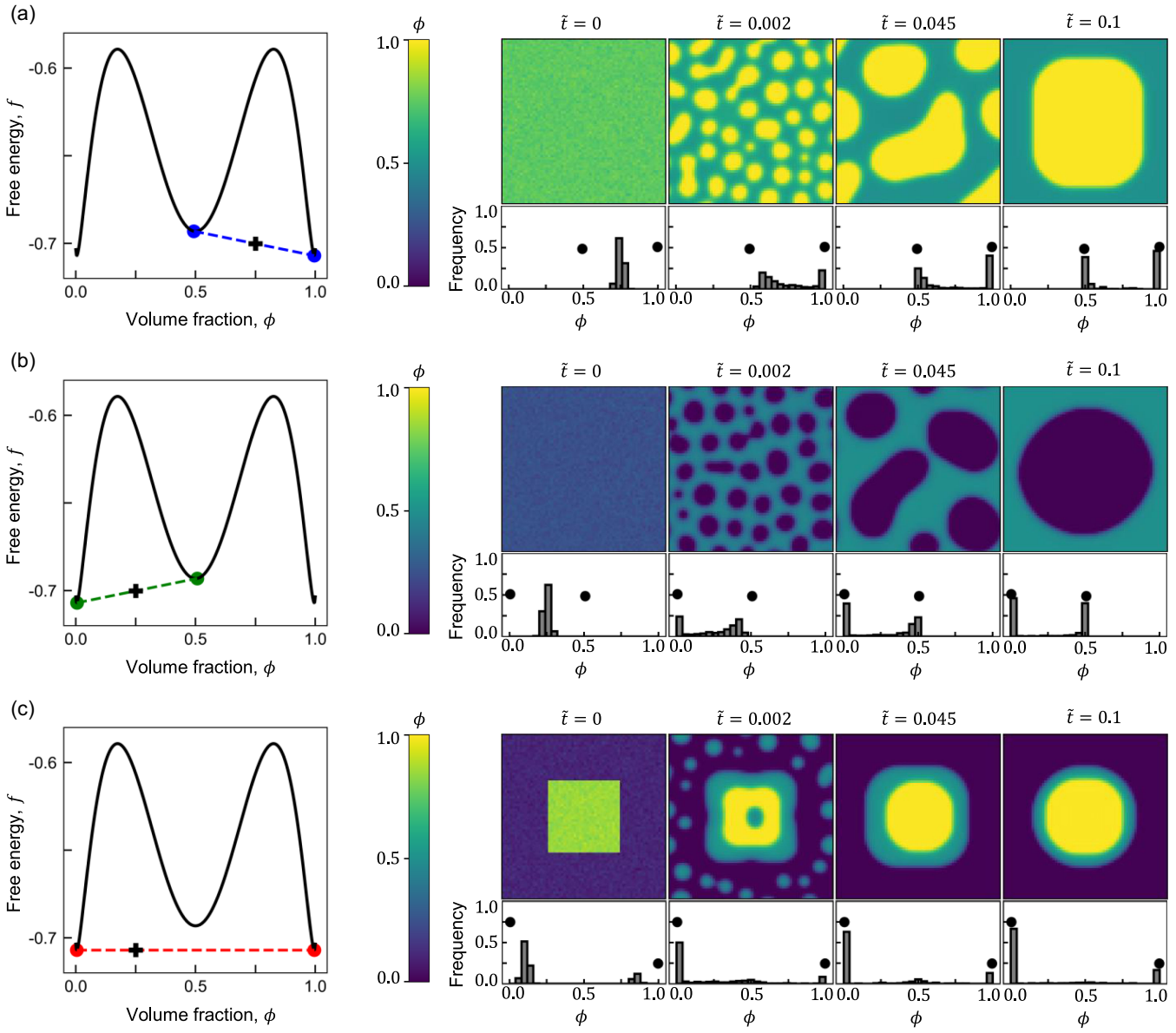


FIG. 4. Phase separation dynamics for a binary mixture with quartic potential. Each panel [(a),(b), or (c)] shows the evolution of the system towards a phase separated state belonging to one of the three possible families (families III, II, and I as described in the main text). Left subpanels show the theoretical predictions, and the right subpanels show numerical solutions of the Cahn-Hilliard Eq. (17). (a) Phase separation into a family III state from an initial homogeneous state with $\phi = 0.75$. Left panel shows the free energy density $f(\phi)$, in units of ν_0^{-1}, with a cross noting the solute volume fraction. Right panels show snapshots of the time evolution of the Cahn-Hilliard equation at different dimensionless times $\tilde{t}$, with histograms of the solute volume fraction below. (b) Same as (a), but the initial state has $\phi = 0.25$, which returns a family II solution. (c) Same as (a), but in this case solute is concentrated in a patch despite an overall value $\phi = 0.25$, which results in a family I solution. Throughout the figure $c = 135$. See also Supplemental Material Sec. S6, S7b, and S7d [32] for further details.

B. Phase separation in continuous space

The approach we have followed so far treats space as a discrete set of compartments. We now numerically investigate the dynamics of phase separation for the model at hand in continuous space by solving a set of equations analogous to the Cahn-Hilliard equations [46] (see Appendix E). In brief, we generalize the composition vectors of the solutes across compartments into vector fields in space, $\boldsymbol{r}$, and time, t, i.e., $\vec{\phi}^{(c)} \to \vec{\phi}(\boldsymbol{r}, t)$. For the case at hand we simply have one composition field, and its time evolution is given by

$$\frac{\partial \phi(\boldsymbol{r}, t)}{\partial t} = \ell \nabla^2 \bar{\mu}(\boldsymbol{r}, t), \tag{17}$$

where ∇ is the gradient towards $\mathbf{r}$. Here, ℓ is a response coefficient, sometimes called mobility, and $\bar{\mu}(\boldsymbol{r}, t)$ is a

generalization of the exchange chemical potential into continuous space, which takes the form

$$\bar{\mu}(\mathbf{r},t) = -\frac{c}{3}\left(\phi - \frac{1}{2}\right)^3 + \log\left(\frac{\phi}{1-\phi}\right) - k\nabla^2\phi. \quad (18)$$

The coefficient k determines the width of the interfaces and is related to the surface tension (see Supplemental Material Sec. S6 [32] for a nondimensional formulation).

Figure 4 shows the dynamics of phase separation for a fixed value of the interaction parameter c. In Panels (a) and (b), the liquid mixture is initially prepared into a homogeneous state with some spatial white noise. For such general initial conditions the system relaxes towards a phase separated state that is metastable and not globally stable. In panel (a), with high solute volume fraction, the phase separated state belongs to family III; and in panel (b), with low solute volume fraction, the system relaxes towards a phase separated state of family II. Note that in both cases the thermodynamic equilibrium is a phase separated state of family I.

Panel (c) shows an example of an initial state that relaxes towards the equilibrium phase separated state, which is a state of family I. Note that the initial condition is a specific one for which the solute is concentrated in one region. The transient dynamics is interesting. Initially, different spatial regions of the liquid mixture appear to evolve towards phase separated states in the families II and III. However, ultimately the regions of intermediate volume fraction shrink, and the system reaches a phase separated state that is a global free energy minimum.

To conclude, we have shown the emergence of metastable phase separation in a simple model of a binary mixture with a quartic interaction energy. The numerical results in Fig. 4 indicate that metastable phase separated states are easier to access than the global equilibrium state. This example thus shows the relevance of metastable phase separated states, in accordance with previous studies [41,42,44,47]. This phenomenology is similar to the one observed in in-vitro experiments with prion-like proteins [24–27], and we elaborate on this in the discussion further.

VI. METASTABLE PHASE SEPARATION IN HOPFIELD LIQUIDS

We next apply the framework for metastable phase separation to the liquid Hopfield model. This model represents a liquid mixture with a large number of components that can encode in their interactions a large number of phases with prescribed compositions. The study of such mixtures is interesting from an engineering point of view with the aim of building synthetic liquids capable of information retrieval [48,49], and as a toy model for biological mixtures, such as the cytoplasm, that have many components and demix into condensates with specific composition [5]. The liquid Hopfield model has been studied in the grand-canonical ensemble [11], and the conditions for the stability of a single phase with a prescribed composition have been determined. However, the problem of multiphase coexistence and separation dynamics in such a model has not yet been discussed. Here, using the formalism derived in this paper, we study metastable phase separation in the liquid Hopfield model.

A. Definition of the liquid Hopfield model

We begin the model definition by specifying the compositions in the target phases. We consider p target vectors $\vec{\xi}^{(\alpha)}$ with $\alpha = 1, \ldots, p$ a label identifying the different targets. The target vectors prescribe whether component i should be enriched ($\xi_i^{(\alpha)} = 1$) or depleted ($\xi_i^{(\alpha)} = 0$) in phase α. For simplicity, we assume that the total number of components enriched in each target phase is the same, i.e., $\sum_{i=1}^{N} \xi_i^{(\alpha)} = Q$ with Q an α-independent constant. In this case, we can define normalized target vectors $\vec{\gamma}^{(\alpha)} = (\vec{\xi}^{(\alpha)} - q)/n$, where $q = Q/N$ is the sparsity parameter and $n = \sqrt{q(1-q)}$ is a normalization factor. By construction, the normalized target vectors satisfy $\vec{\gamma}^{(\alpha)} \cdot \vec{1} = 0$ and $\vec{\gamma}^{(\alpha)} \cdot \vec{\gamma}^{(\alpha)} = N$, where $\vec{1}$ is the vector of all unit entries.

In the liquid Hopfield model the affinity matrix J_{ij}, which specifies the energy u in Eq. (5), takes a particular form, so that the liquid demixes into phases of prescribed compositions. Following [11,22,50], J_{ij} is defined as the orthogonal projector on the linear space spanned by the p normalized target vectors $\vec{\gamma}^{(\alpha)}$:

$$J_{ij} = \sum_{\alpha=1}^{p} \gamma_i^{(\alpha)} M_{\alpha j}, \quad (19)$$

where $M_{\alpha j}$ is the pseudo-inverse (also known as the Moore-Penrose inverse) of the matrix $\gamma_i^{(\alpha)}$ [51,52]. In the specific case when the p target vectors $\vec{\gamma}^{(\alpha)}$ are linearly independent, we have that

$$M_{\alpha j} = \sum_{\beta=1}^{p} c_{\alpha\beta}^{-1} \gamma_j^{(\beta)}, \quad (20)$$

where $c_{\alpha\beta} = \sum_{i=1}^{N} \gamma_i^{(\alpha)} \gamma_i^{(\beta)}/N$ is the pattern covariance matrix [53,54]. Inserting Eq. (20) into Eq. (19) we recover the form in [11] for J_{ij}. Notice that the inverse of $c_{\alpha\beta}$ does not exist when the targets are not linearly independent.

Besides the pairwise affinity term, in Ref. [11] it was shown that the presence of higher order nonlinearities enables stability of target states. We therefore use the simple diagonal form

$$K_{ijk} = N^2 \delta_{ij} \delta_{jk} \quad (21)$$

for the cubic term in Eq. (5), and set all remaining terms to zero. Note that the N scaling of J_{ij} and K_{ijk} is such that the quadratic and cubic contributions to the free energy are of the same order of magnitude.

For simplicity we consider the case for which the total volume fraction occupied by each of the i solute components are identical, i.e., $\phi_i = \phi/N$.

B. Stationarity of phase separated retrieval states

To investigate metastable phase separation in the liquid Hopfield model, we first consider phase separated states with two compartments ($C = 2$). Later, at the end of the section, we discuss the case with $C > 2$.

Let us consider a mixture for which one compartment has an enrichment profile that is similar to the target state α. Thus, in this compartment components with $\xi_i^{(\alpha)} = 1$ are enriched and components with $\xi_i^{(\alpha)} = 0$ are depleted, where α is one of the p prescribed target compositions. We label the phase corresponding with this compartment by α, and its compartment volume is denoted by $w^{(\alpha)}$. Because of conservation of component abundances, the second compartment, labeled by $-\alpha$, is conversely enriched in the components with $\xi_i^{(\alpha)} = 0$ and depleted in those with $\xi_i^{(\alpha)} = 1$. In what follows, we call α the "*αth retrieval phase*" and we refer to $-\alpha$ as its "*anti-retrieval phase*." We call the phase separated state consisting of a pair of phases, one retrieval and the other antiretrieval, *the retrieval state*.

We focus for now on the simple case for which $q = 1/2$, while the general case of arbitrary q is discussed in Appendix F. For $q = 1/2$, if a certain amount of a component is enriched in a retrieval phase, the exact same amount is depleted in its antiretrieval phase. Thus, the compositions of an αth retrieval phase are given by

$$\phi_i^{(\alpha)} = \frac{\phi}{N}(1 + a\gamma_i^{(\alpha)}), \tag{22}$$

and those of its antiretrieval phase are

$$\phi_i^{(-\alpha)} = \frac{\phi}{N}(1 - a\gamma_i^{(\alpha)}). \tag{23}$$

In the expressions (22) and (23), a is the *overlap parameter* of the retrieval phase that quantifies the quality of retrieval. The quality of retrieval of an arbitrary composition vector $\vec{\phi}$ is determined by the p *overlap observables*

$$a^{(\nu)}(\vec{\phi}) = \frac{\vec{\gamma}^{(\nu)} \cdot \vec{\phi}}{\vec{1} \cdot \vec{\phi}} \tag{24}$$

with $\nu = 1, 2, \ldots, p$. If the targets $\gamma^{(\alpha)}$ are orthogonal, then the retrieval phase $\vec{\phi}^{(\alpha)}$ satisfies

$$a^{(\nu)}(\vec{\phi}^{(\alpha)}) = a\,\delta_{\nu,\alpha}. \tag{25}$$

Therefore, $a = 0$ corresponds to a homogeneous state, i.e., no retrieval; $a \in (0, 1)$ to retrieval, i.e., components present in the target have higher densities than those absent in the target; and $a = 1$ corresponds to full retrieval, i.e., the components with $\xi_i^{(\alpha)} = 0$ have been completely removed from the phase. If the $a^{(\nu)}$ are nonzero for multiple values of ν, then we speak of a *spurious state*.

Using Eqs. (22) and (23) in the constraint for the compositions, Eq. (9), we find that both phases have equal volume,

$$w^{(\alpha)} = w^{(-\alpha)} = 1/2, \tag{26}$$

which is a consequence of the symmetry of the model. Instead, for $q < 1/2$ the two compartments have different volumes (see Appendix F).

Next, we demonstrate that a phase separated state consisting of a pair of phases, α and $-\alpha$, that have equal volumes is stationary if the overlap parameter a takes on a specific value a^*. To this aim, we apply the stationarity conditions, Eqs. (10) and (11), to the phase separated state. The exchange chemical potentials of the components in each of the compartments are given by

$$\bar{\mu}_i^{(\pm\alpha)} = \mp v_2\phi a\gamma_i^{(\alpha)} + \frac{v_3\phi^2}{2}\left(1 \pm a\gamma_i^{(\alpha)}\right)^2 + \log(\phi(1 \pm a\gamma_i^{(\alpha)})) - \log(1-\phi) - \log(N), \tag{27}$$

and the corresponding osmotic pressures are

$$\Pi^{(\pm\alpha)} = \frac{v_2\phi^2 a^2}{2\nu_0} - \frac{v_3\phi^3}{3\nu_0}(1 + 3a^2) + \frac{1}{\nu_0}\log(1-\phi). \tag{28}$$

One can then show that if $a = a_*$, with a_* the solution to

$$a_* = \tanh(a_*\phi(v_2 - v_3\phi)), \tag{29}$$

then the stationarity conditions $\bar{\mu}_i^{(\alpha)} = \bar{\mu}_i^{(-\alpha)}$ and $\Pi^{(\alpha)} = \Pi^{(-\alpha)}$ are satisfied for the above expressions of $\bar{\mu}_i^{(\pm\alpha)}$ and $\Pi^{(\pm\alpha)}$.

Notice that the stationary compositions of the two phases α and $-\alpha$ are the same as those found previously in the grand canonical setup [11]. However, here we consider a spatially heterogeneous state consisting of two phases, while Ref. [11] studied homogeneous states consisting of one phase. Furthermore, here the volume fraction ϕ is an external control parameter, whereas in the grand canonical ensemble it is a variable that is determined by the chemical potentials of the reservoirs. The coexistence of phases α and $-\alpha$ is here a consequence of particle conservation. Nevertheless, the fact that these two phases are local minima of the grand potential is a consequence of the

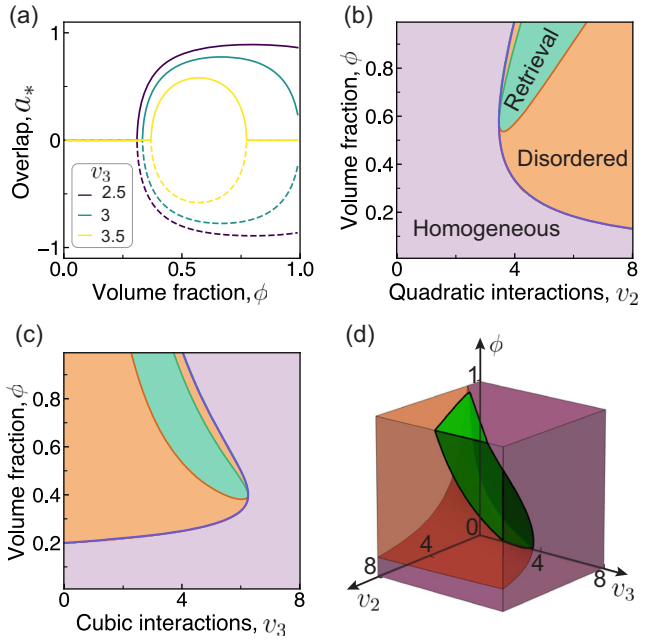


FIG. 5. Stationarity and stability diagrams of the liquid Hopfield model. (a) Overlap a_* as a function of the volume fraction ϕ, for different values of the cubic interaction v_3 and at fixed $v_2 = 4$. The onset of nonzero overlap indicates the emergence of stationary target states. The quantity a_* is obtained by solving Eq. (29). (b). Spinodal lines in the (v_2, ϕ) plane, delimiting regions where either the homogeneous state (violet) or all retrieval phases (green) are stable and for fixed $v_3 = 3$. In the orange region neither the homogeneous nor the retrieval states are stable. The curves drawn correspond to solving the equations obtained by replacing the inequalities in Eqs. (31) and (30) by equalities. (c) Same as (b). but in the (v_3, ϕ) plane for fixed $v_2 = 4$. (d) Schematic representation of the stability diagram in the v_2, v_3, ϕ space. For clarity, the small region between the homogeneous and retrieval region was omitted.

symmetry of J_{ij}, and also occurs in the Hopfield model for associative memory [22].

Figure 5(a) shows the solutions to Eq. (29) as a function of ϕ. The plot shows that the liquid mixture has stationary phases that successfully retrieve the prescribed phases if

$$\phi(v_2 - v_3\phi) > 1. \tag{30}$$

There is an intermediate value of the volume fraction ϕ for which the overlap a, and thus the quality of retrieval, is maximal. Notice that Fig. 5(a) does not show the typical first order phase transition of liquid mixtures, as it is a plot of the stationary state. To study phase transitions we should analyze the stability of the resultant phase, and as will become evident, near the transition line $\phi(v_2 - v_3\phi) \approx 1$ the stationary phase is not stable.

We finally remark that the liquid Hopfield model also admits stationary states with $C > 2$ that consist of multiple pairs of retrieval and anti-retrieval phases. In particular, a phase-separated state composed of multiple pairs of stationary phases, with compositions $\vec{\phi}^{(\alpha)}$ and $\vec{\phi}^{(-\alpha)}$ as given by Eqs. (22) and (23), and with compartment volumes satisfying $w^{(\alpha)} = w^{(-\alpha)}$ (but otherwise arbitrary), is stationary provided that $a = a^*$ holds for all pairs of retrieval–antiretrieval phases. Next, we study the stability of these states.

C. Metastability of homogeneous and phase separated retrieval states

The homogeneous state is metastable if the Hessian of its free energy is positive. As derived in [11], the spinodal of the homogeneous state is attained when Eq. (30) becomes an equality. The parameter region for which the homogeneous state is metastable is indicated with a purple shade in Figs. 5(b)–5(d). For fixed parameters ϕ, the homogeneous state gets unstable at large enough values of v_2, which represents the onset of phase separation [see Figs. 5(b)]. A metastable retrieval region exists for large enough values of ϕ and for a certain parameter range of the interactions v_2 and v_3, which have to be positive but not too large.

As we demonstrated in Sec. IV, stationary phase separated states are metastable provided all constituent phases are stable. For the liquid Hopfield model sufficient conditions for the stability of any retrieval phase were derived in Ref. [11] and are given by

$$\phi(1 + a_*)(v_2 - v_3\phi(1 + a_*)) \leq 1, \tag{31}$$

$$\phi(1 - a_*)(v_2 - v_3\phi(1 - a_*)) \leq 1, \tag{32}$$

where a_* solves Eq. (29) (see Appendix G for a generalization to arbitrary q). Therefore, a retrieval state consisting of two phases, $P = 2$, is metastable provided these conditions are met for the pair of retrieval and antiretrieval phase that it is composed of. We emphasize that the conditions (31) and (32) are sufficient, but not necessary, for metastability. In general, the stability of retrieval phases is different for each choice of the targets $\{\vec{\xi}^{(\mu)}\}_{\mu=1,\ldots,p}$ encoded by J_{ij}. Furthermore, the stability of a particular retrieval phase depends on the retrieved target α. Nevertheless, as it was shown in Ref. [11], the sufficient conditions above become also necessary when p is large enough.

Figures 5(b)–5(d) show the region in parameter space for which phase separated retrieval states are stable (indicated with the green shade). In this region, all p encoded retrieval states are stable, provided that these retrieval states are linearly independent, and thus $p \leq N - 1$. Note that stability of retrieval states requires a repulsive cubic interaction, in agreement with the findings in Ref. [11]. Figures 5(b)–5(d) also show a region in which neither the homogeneous nor the retrieval states are stable. In the

previous work [11] this region was called the disordered region, as the stable configurations in this region have little resemblance with the prescribed compositions.

For $C > 2$, the liquid Hopfield model can simultaneously retrieve multiple pairs of stationary retrieval, antiretrieval phases, $(\vec{\phi}^{(\alpha)}, \vec{\phi}^{(-\alpha)})$, corresponding with different target compositions α. In this case, the stationary configurations are not metastable, as they can have soft modes (see Sec. IV). Indeed, if we vary the volumes of the different phases with the constraint $\sum_{\alpha=1}^{P} w^{(\alpha)} = \sum_{\alpha=1}^{P} w^{(-\alpha)}$ maintained, where P indicates the number of retrieved target compositions, then we obtain phase separated states with the same free energy as the original configuration. Thus, the local minimum of the free energy is in fact a metastable plateau. A possible way to stabilize such a configuration is by introducing a nonzero surface tension, as we do in the following section. Because of surface tension, the number of interfaces should be minimized, and therefore only the state within the metastable plateau that has the minimal surface tension will remain metastable when including surface tension into the model.

D. Information retrieval via nucleation of retrieval phases

So far we have shown that the liquid Hopfield model admits a parameter regime in which all retrieval phases are metastable [green shaded area in Fig. 5(b)–5(d))]. However, this is not sufficient to demonstrate that Hopfield liquids can reliably nucleate the stored phases from a partial cue of information, i.e., from a region in space with compositions that have some similarity with a target state. Indeed, the free energy of the liquid Hopfield model may have metastable spurious states that disrupt the relaxation towards the desired target phases. Therefore, in this section we investigate the nucleation ability of Hopfield liquids by studying their dynamics in continuous space.

Our starting point is the Cahn-Hilliard equations for a multicomponent mixture,

$$\frac{\partial \phi_i(\mathbf{r}, t)}{\partial t} = \ell \nabla^2 \bar{\mu}_i(\mathbf{r}, t), \tag{33}$$

with the spatially dependent exchange chemical potentials given by

$$\bar{\mu}_i = \nu_0 \left(\frac{\partial f}{\partial \phi_i} - k \nabla^2 \phi_i \right); \tag{34}$$

see Appendix E for a more detailed exposition. These equations describe the dynamics of a multicomponent mixture in continuous space. We then consider an initial condition that is slightly biased towards one of the target compositions, and thus acts as a partial information cue. Starting from this initial condition, we investigate whether the system nucleates the retrieval phases described by the Eqs. (22) and (23).

The partial cue, which acts as nucleation seed, consists of a small patch enriched (or depleted) in some (but not all) the components of the target composition. Besides this small patch the remaining space is a homogeneous mixture. Figures 6(a) and 6(b) show that the Hopfield liquid indeed evolves towards a phase separated state with two phases ($P = 2$). The final stable phases are precisely the retrieval and antiretrieval phases that match with the initial cue provided. We find successful nucleation for all the p targets that are stored in the affinity matrix of the Hopfield liquid (in this example $p = 3$, see also Supplemental Material Fig. S5 [32]). Thus the different retrieval phases are simultaneously metastable and can be nucleated reliably by choosing a proper initial cue. Importantly, the initial cue does not have to be complete, which demonstrates that Hopfield liquids function properly as liquid analogs of associative memories.

The snapshots in panels (c) and (d) of Fig. 6 show the same dynamics as panels (a) and (b), but the coloring scheme uses the local overlap observables, $a^{(\nu)}(\vec{\phi}(\mathbf{r}))$ [see Eq. (24)]. This allows us to visualize nucleation of retrieval phases as the appearance of a uniformly colored phase (see details of coloring scheme in the caption). At long times, the numerical solution approaches the analytically computed values for the overlaps, $a^{(\nu)}(\vec{\phi}^{(\alpha)}) = \pm a_* \delta_{\alpha,\nu}$, corroborating the theory. Therefore, Hopfield liquids are capable of information retrieval from partial cues, in agreement with theoretical predictions.

E. Metastable phase separation in multicomponent mixtures

We have shown that Hopfield liquids are multicomponent mixtures that can reliably retrieve phases with prescribed compositions via nucleation seeds that have partial information on the target phases. In this section, we study how the liquid Hopfield model spontaneously phase separates into multiple phases with distinct, prescribed compositions, and thus serves as a toy model for how the cytoplasm demixes through liquid-liquid phase separation into multiple biomolecular condensates.

Figure 7 shows the dynamics of a Hopfield liquid in the region of parameter space for which stationary retrieval states are stable. As in the previous section, we consider here the case $N = 8$ and $p = 3$. The system is initialized in a state that is spatially homogeneous, with a small spatially fluctuating perturbation [see panel (a)].

As the system evolves over time, the components start to spatially segregate, so that the densities of particular components are enhanced in different spatial regions. This phase separation process can be seen in panel (b) [see panel (e) for the coloring scheme]. Since $q = 1/2$, the phases are not pure, but rather complex mixtures enriched and depleted in specific components.

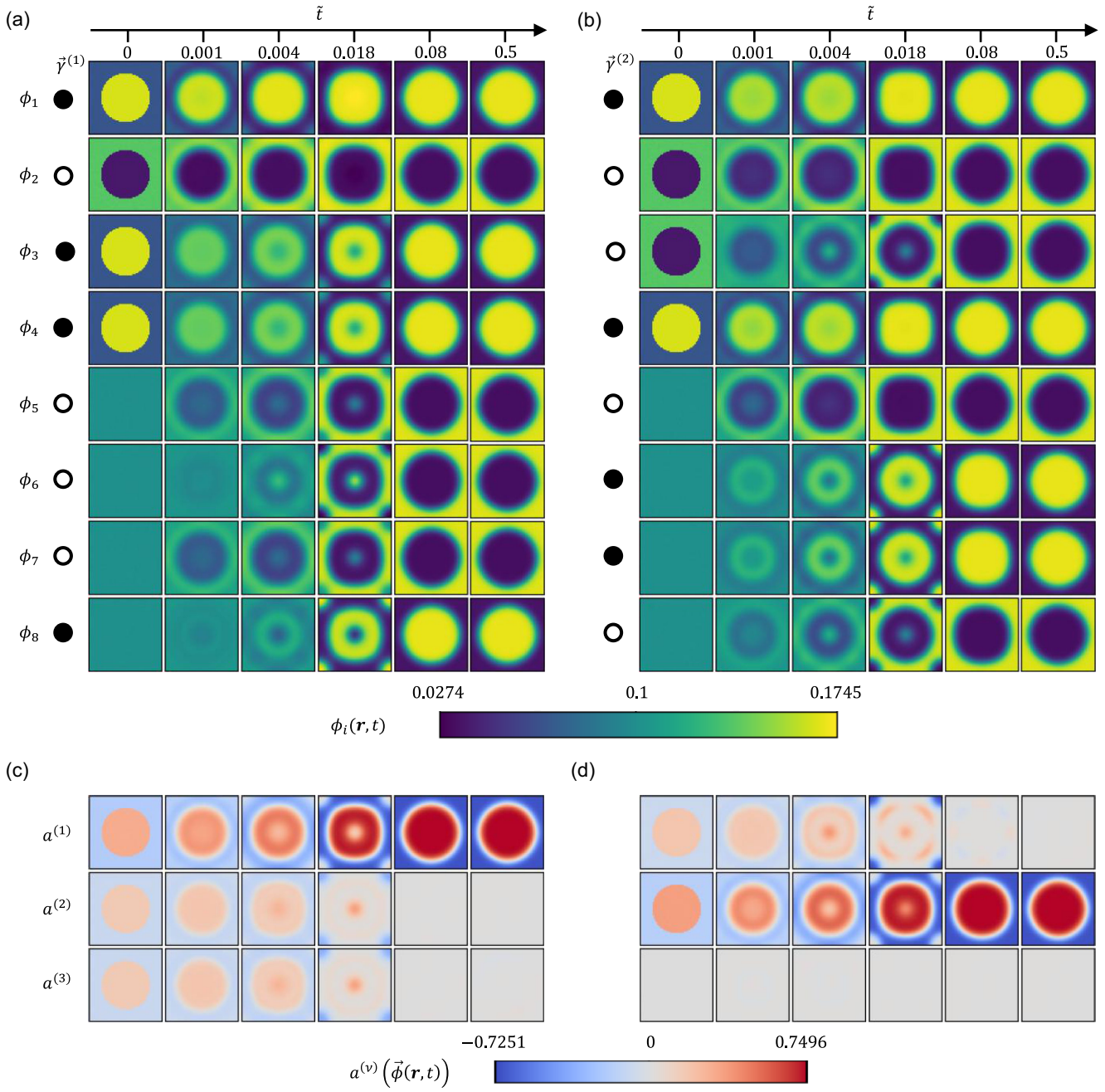


FIG. 6. Retrieval of information from a partial cue in the liquid Hopfield model. (a) Snapshots of the retrieval dynamics of the compositions, $\phi_i(\mathbf{r},t)$, obtained from solving the Cahn-Hilliard Eqs. (33)–(34) for the liquid Hopfield model when it stores three targets. The initial state has a small seed that overlaps with target $\alpha = 1$ only in components $i = 1,\ldots,4$. As time progresses the system relaxes to the target phase separated state. (b) Same as (a), including same targets encoded in the interaction matrix J_{ij}, but the initial condition is set so that the first four components match target $\alpha = 2$. The system thus relaxes to the retrieval phase separated state $\alpha = 2$. (c). The three local overlaps $a^{(\nu)}(\vec{\phi}(\mathbf{r},t))$ with $a^{(\nu)}$ defined in Eq. (24) and for $\vec{\phi}$ from panel (a). (d) Same as (c), but with the compositions of panel (b). The model parameters used in the figure are $v_2 = 4$, $v_3 = 3$, $\phi = 0.8$. Further details can be found in Supplemental Material Sec. S7d [32]. Three targets are encoded in J_{ij}, from which two are shown, and the third is $\vec{\gamma}^{(3)} = (+-+-++--)$ (see Supplemental Material Fig. S5 [32]).

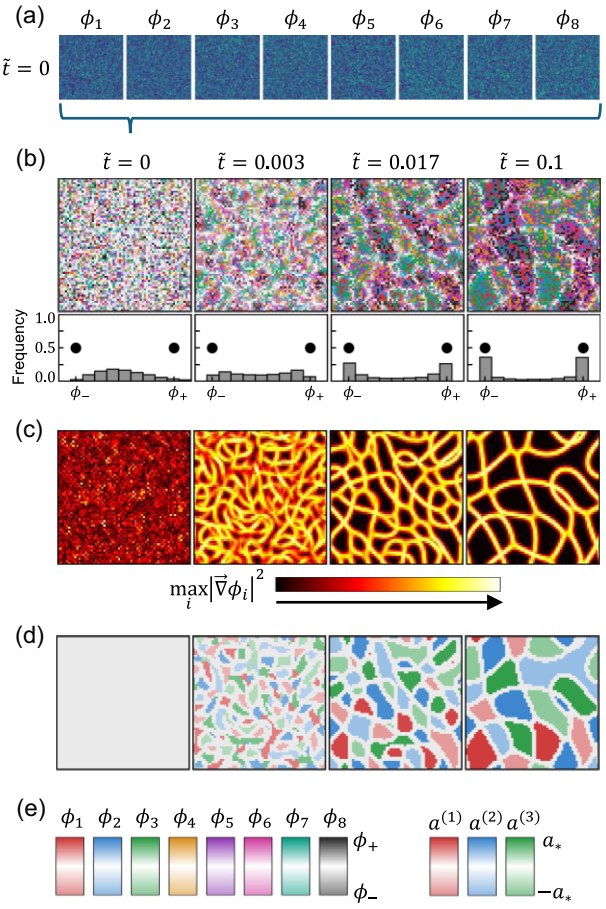


FIG. 7. Nucleation and coexistence of multiple target phases from a random initial condition. (a) Initial compositions are spatially uniform with $\phi_i = 0.1$, plus a small noise perturbation. Color bar as in Figs. 6(a) and 6(b). (b) Time evolution of the density fields. Each pixel is colored according to the largest density field at that point [color bars in panel (e)]. Visually, the emergence of different domains is apparent. The histograms show how the density fields approach the values ϕ_+ and ϕ_-, where we have defined $\phi_\pm = \phi/N(1 \pm a^*)$. (c) Time evolution of interfaces. The panels show the heatmaps of $\max_i |\nabla\phi_i|^2$. With increasing time, the percentage of interface points decreases. The arrow below the color bar indicates increasing values of the gradient. (d) Nucleation of target phases identified by the algorithm in Supplemental Material Sec. S7c [32]. Phases are colored according to the maximum overlap with the targets. Interface points are left gray. (e) Color bars used in panels (c) and (d). Parameters as in Fig. 6, see also Supplemental Material Sec. S7d [32].

To systematically identify the different phases present in the system at a given time, we follow the approach developed in Refs. [55,56]. In brief, the method uses the gradient of the compositions, shown in panel (c), to determine domain interfaces, and then identifies the composition of phases among the domains (see Supplemental Material Sec. S7c [32]). In panel (d), each of the identified phases is colored based on the value of the largest (or lowest) overlap with one of the targets. As one can see, as time progresses the amount of interface is reduced (see detailed analysis in Supplemental Material Fig. S6 [32]), and the domains become larger. Importantly, the overlaps with the targets increase over time (the colors become more vivid).

F. Retrieval capacity of Hopfield liquids

We now investigate the number of target phases that a liquid mixture with N components can successfully retrieve. For associative neural networks it is known that the number of patterns that can be reliably retrieved increases proportionally with the number of neurons [31,57]. In Sec. VI C we showed that the liquid Hopfield model can store up to $N - 1$ targets, with all of them being simultaneously stable. However, Hopfield liquids also admit spurious phases, and therefore it remains to be addressed whether the target phases are retrievable under physical dynamics.

In order to measure the retrieval capacity of the liquid Hopfield model, we numerically solve the Cahn-Hilliard equations for several values of p and N starting from a random initial condition. We consider here orthogonal targets, so that the phase identification algorithm separates them easily (see Supplemental Material Sec. S7d [32] for details on how to generate orthogonal targets). Qualitatively similar results can be obtained for nonorthogonal targets (see Supplemental Material Fig. S7 [32]).

In Fig. 8 [panel (a)] we present the final snapshots of such Cahn-Hilliard simulations. Different phases are identified through the method described in Supplemental Material Sec. S7c [32], which works here well as we have chosen orthogonal targets. Target phases are highlighted with bright colors, whereas nontarget phases are colored with different shades of gray. For $N = 8$, we observe that for $p < 4$ all phases in the final configuration are either retrieval or antiretrieval phases, while for $p \geq 4$ the mixture evolves towards a phase separated state that contains nontarget phases. For larger values of N, reliable retrieval is possible for a larger number of target phases, as the nontarget phases appear at higher values of p. Hence, the retrieval capacity of the liquid Hopfield model increases as a function of the number of components.

To quantify the retrieval capacity of the liquid Hopfield model, we plot in panel (b) the fraction, χ, of demixed phases in the final configuration that correspond to retrieval or antiretrieval phases as a function of p. For each N, χ decays like a sigmoid as a function of p, and thus the fraction of phases that corresponds to the encoded targets decreases as a function of p. Crucially, the midpoint of the sigmoid, $p_{1/2}$, increases linearly with N [see panel (c)]. Figures 8(d) and 8(e) characterize the kinetics of retrieval, which show that as the number of encoded targets increases the dynamics of retrieval becomes slower (see Supplemental Material Fig. S6 [32] for interface dynamics). Taken together, these results

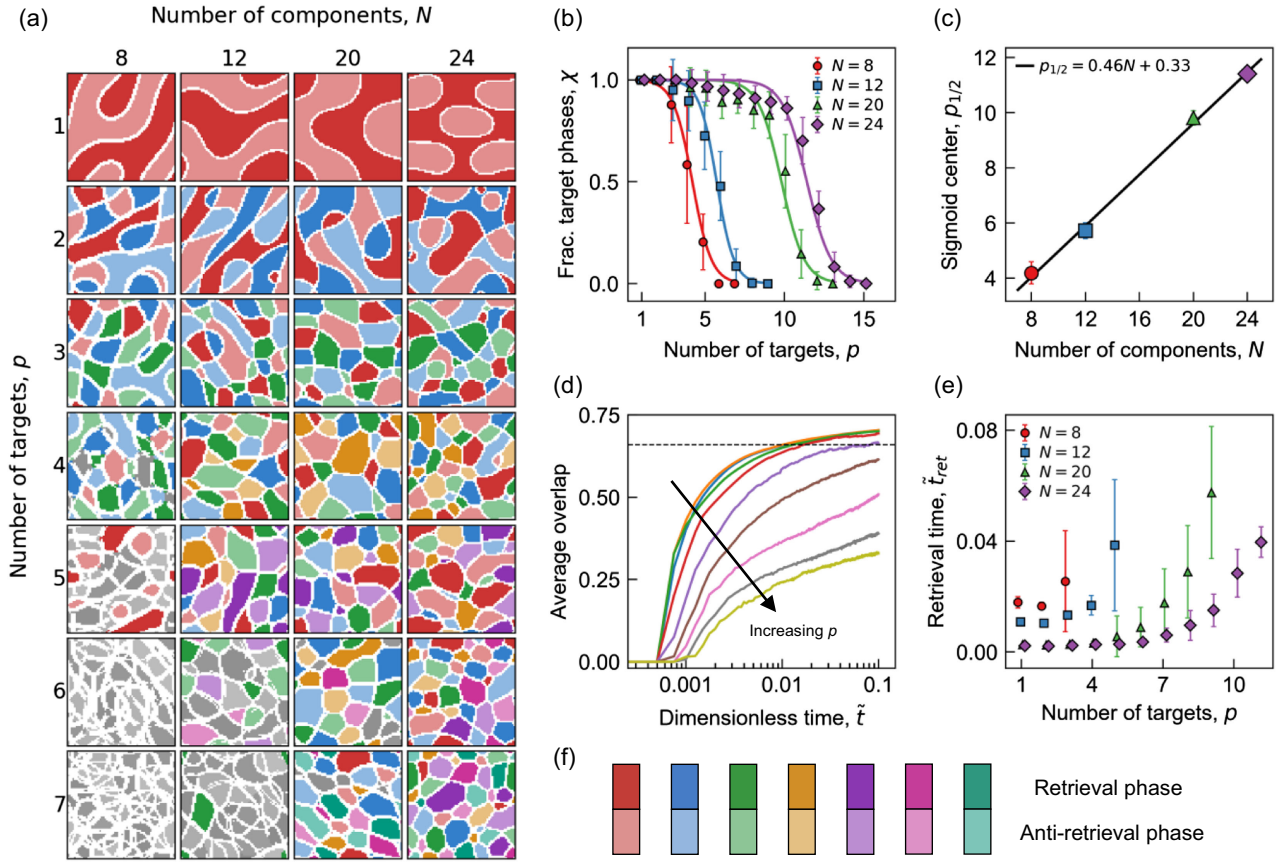


FIG. 8. Retrieval capacity of a Hopfield liquid. (a) Visualization of the phases in the liquid Hopfield mixture in the region where all retrieval phases are stable (green region of Fig. 5). The figure data is obtained from solving Cahn-Hilliard equations for a given number of components N and targets p as indicated in the figure. The phases are identified as regions where the gradients of the $\phi_i(\mathbf{r})$ are small using the procedure described in Supplemental Material Sec. S7c [32]. Phases are visualized with chromatic colors if they are identified as target phases [if the absolute value of the overlap of a phase with a given target is larger than 0.66, i.e., $\simeq 0.9a_*$, the phase is considered a target phase and it is assigned a chromatic color, see panel (f)]. If a phase is not identified as a target phase, then it is given a random shade of gray. Interface points are left white. (b) The fraction of target phases, χ, i.e., the ratio between the number of target phases and the total number of phases in a given configuration, is plotted as a function of p for various values of N as indicated in the legend. Markers are sample averages over the final configurations of 30 Cahn-Hilliard simulations with randomized initial conditions and targets. The solid lines are sigmoid functions $\chi(p) = 1/(1 + \exp[b(p - p_{1/2})])$, where b and $p_{1/2}$ are fitting parameters. (c) The midpoints of the sigmoids in panel (b) (indicated with $p_{1/2}$) are plotted against the number of components N and fitted with a straight line. (d) Average overlap as a function of $\tilde{t}$, for $N = 12$ and increasing values of p (from 1 to 9). For each phase, the overlap is computed with the best-matching stored target, and the average is taken over all phases weighted by their volume fractions (see Supplemental Material Sec. S7d [32] for details). The curves represent averages over 30 independent simulations. The dashed black line indicates the threshold used to identify (anti)retrieval phases in panels (a)–(c), i.e., $0.9a_*$. (e) Retrieval time, $\tilde{t}_{\text{ret}}$, defined as the first time the average overlap exceeds $0.9a_*$, as a function of p for different values of N. Markers are sample averages over 30 Cahn-Hilliard simulations, with error bars representing the sample standard deviation. The retrieval time $\tilde{t}_{\text{ret}}$ increases with p, implying that retrieval dynamics is hindered by the presence of a large number of metastable states. (f) Color scheme for panel (a). The values of the parameters are $\phi = 0.8$, $v_2 = 4$, and $v_3 = 3$. For more figure details check Supplemental Material Sec. S7d [32].

demonstrate that liquid mixtures can retrieve a number of prescribed phases that is extensive on the number of components in the mixture.

VII. DISCUSSION

A. Summary

In this paper, we have derived the conditions for metastability of phase separated states in multicomponent liquid mixtures. We have found that stability of all constituent phases is necessary and sufficient for stability of the phase separated state, with only singular exceptions. To illustrate this, we developed a minimal model for metastable phase separation in a binary mixture with highly non-linear interactions. Furthermore, studying the liquid Hopfield model in the canonical ensemble, we have shown that multicomponent liquid mixtures can phase separate into phases of prescribed compositions and thus perform

reliable information retrieval through nucleation. Therefore, this latter model can be seen as a toy model for cytoplasmic organization through phase separation or phase separation in synthetic multicomponent mixtures.

B. Relation to prior theoretical studies

Theoretical research on multicomponent liquids can be broadly divided into two lines of research: the direct approach and the inverse approach. In the direct approach, the affinity matrix J_{ij} in Eq. (5) is defined as a random matrix. Investigation then focuses on either characterizing the spinodal manifold, see Refs. [12,14,58–60], which can be done analytically using random matrix theory; or on characterizing the low temperature phase separated states [13,56,61,62], which can be done numerically via simulations. In the inverse approach, the compositions of the different phases are prescribed, and the choice of the affinity matrix J_{ij} is such that the prescribed phases are stable. This approach has been investigated through numerical optimization of J_{ij} in Refs. [15,61,63].

In contrast to these works, our paper solves the inverse problem analytically by studying the liquid Hopfield model in the canonical ensemble. We exploited the structure of a Hebbian J_{ij} to analytically characterize metastable phase separated states that correspond to the prescribed compositions. Crucially, such states can be enriched in a large number of components, $Q \sim N$, so that in the limit $N \gg 1$ an arbitrary pair of targets share a finite fraction of components. In contrast, Refs. [61,63] studied the case in which for $N \gg 1$ a pair of targets do not share components, see also discussion in Ref. [11]. Moreover, we were able to simulate the spatial dynamics of a mixture with a large number of components (up to $N = 24$) and obtain results that precisely agree with our theoretical predictions.

In order to achieve such an accurate picture of demixing in multicomponent liquids, we first developed the general formalism of metastable phase separation. Metastability has been observed in experiments [24–27], discussed analytically in the grand canonical ensemble (in the case of a single phase) [11], explored in numerical studies of phase separation [15,56], and its role in the phase separation dynamics in a variety of contexts has been recognized since long ago [41,42,44,47]. However, the mathematical conditions for metastable phase separation had so far not been derived. These conditions are useful for verifying whether the phase separated states obtained from numerical algorithms, such as the one in Ref. [15], are metastable, and not saddles in a high-dimensional landscape. The result that metastability of a phase separated state is, excluding the (peculiar) case of emergent soft modes, equivalent to metastability of all constituent phases is simple yet powerful.

C. Relation to experimental work

We discuss three lines of experimental research related to our work: metastability of biomolecular condensates, principles of cytoplasmic organization, and synthetic liquids.

Multiple papers have shown that solutions of prion-like proteins or peptides can rapidly phase separate into liquid droplets [24–27]. However, after several hours, these droplets transition to a distinct aggregate phase, indicating that the droplets are metastable. The binary mixture model in Sec. V constitutes a toy model for such experiments. In particular, Ref. [26] shows that in the metastable state medium-density and high-density liquid phases coexist, whereas in the stable state a low-density liquid phase coexists with a high-density aggregate phase. Such results are consistent with those in Fig. 4, although the dense phase in our model is liquid. Overall, our thermodynamic framework is a first step towards quantifying metastable phase separation in these experimental systems.

The cellular cytoplasm is a mixture with a large number of components that encodes condensates of precise composition, see, e.g., [7]. The same network of protein interactions that allows for condensates to phase separate under particular conditions, also allows for multiple condensates to coexist with each other. The results in Sec. VI show that Hopfield liquids are multicomponent mixtures that exhibit both these features, see Figs. 6 and 7, respectively, and therefore constitute a toy model of the cytoplasm. It remains open how to relate this model to empirically determined protein interaction networks [4,64,65].

Our work also relates to synthetic multicomponent mixtures, which can be designed using DNA technology [49,66,67]. In particular, recent work has demonstrated how DNA nanostar sequences can be designed so that the interaction matrix of nine different components enables phase separation into nine liquid phases, each enriched in a single component [49]. A conceptually straightforward, but technically challenging, next step is to find sequences that encode the interaction matrix in Eq. (19), instead of the diagonal interaction matrix studied in [49]. This would allow the creation of a Hopfield liquid, in which multiple phases with prescribed composition share components with each other.

D. Extensions of Hopfield liquids

We have studied metastable phase separation in a minimal version of the liquid Hopfield model. In Ref. [11] we showed that several aspects of the model can be generalized, without altering its essential behavior. As an example of a model extension, in Appendix F and Supplemental Material Sec. S8 [32] we study the effect on phase separation of having the target compositions enriched in $Q < N/2$ components. We find that, unlike for the case $Q = N/2$, for $Q < N/2$ the retrieval and anti-retrieval phases have different volumes $[w^{(\alpha)} < w^{(-\alpha)}$, see

Supplemental Material Fig. S8 [32]]. We have run Cahn-Hilliard simulations to test these predictions for the particular case of $N = 20$, $p = 1$, and $q = 2/5$. The simulations give results in good agreement with theoretical predictions (see Supplemental Material Fig. S9 [32]). Furthermore, we have numerically investigated the case of a nonequimolar mixture, i.e., a mixture in which the abundances of the solutes are not necessarily all equal. In particular, we have performed simulations for different values of the standard deviation of the ϕ_i's (up to roughly 67% of the average value ϕ/N). The results show how, with increasing heterogeneity in the abundances of the solutes, the probability of successful retrieval decreases, whereas the asymmetry between retrieval and antiretrieval phases increases (see Supplemental Material Fig. S10 [32]). These phenomenologies are more similar to those of biomolecular condensates. Model extensions can also be aimed at finding alternative ways of stabilizing Hopfield phases. In the main text we used a cubic repulsive interaction to stabilize phase-separated retrieval phases, an idea originally proposed in Ref. [11] and later also explored in [68]. Next, we propose three alternative approaches to stabilize demixing of Hopfield phases.

First, it is possible that chemical reactions can be used to stabilize retrieval phases. Indeed, chemical dissipation is known to unfold a large class of different behaviors in liquid phase separation [59,69–72], including phase stabilization. Moreover, retrieval of target structures far from equilibrium has already been realized for solid assemblies [73,74]

Second, the surface energy tensor, taken as diagonal in Appendix E, may also be exploited to stabilize retrieval phases in Hopfield liquids, in the spirit of the Ref. [75]. Indeed, as we show in Supplemental Material Sec. S10 [32], at $v_3 = 0$ there exists a region of parameter space for which the only unstable mode of the phase separated target state is one that creates a new interface. Therefore, a strong and programmable surface energy tensor may stabilize retrieval phases in absence of cubic nonlinearities.

Third, an interaction matrix J_{ij} different from the Hebbian matrix proposed here may result in stable Hopfield phases. Alternatives to the Hebbian rule have been numerically studied in [63,76], which did not include cubic interactions. However, the $N \to \infty$ scaling there studied applies to the limit $q \to 0$, in which phases do not share components with each other, see the discussion in Ref. [11]. Indeed, strong nonlinearities are a generic requirement of neural networks to adequately perform computations [77,78]. It remains nonetheless an open mathematical question whether the entropic nonlinearities suffice to stabilize Hopfield phases for an alternative J_{ij} in the limit of large N and nonzero q.

E. Perspective

Biological systems are characterized by a high dimensional interaction space. The naïve expectation for this scenario is that disorder dominates biological matter [12,13]. Nevertheless, ordered structures emerge across biological scales: proteins fold into well-defined conformations [79], folded proteins bind specifically to form multimeric assemblies [80], and assemblies are often concentrated into liquid condensates [81]. From the biological viewpoint this should not come as a surprise, since biological interactions are evolved so that ordered structures perform specific functions. However, from the physics point of view, finding the rules behind this multifarious state of matter is an exciting and challenging endeavor [11,82,83].

From a physics point of view, we have shown how multicomponent liquids are capable of two fundamental information processing tasks: pattern completion and information storage. To do so, we have built upon the (imperfect) mathematical equivalence between multicomponent mixtures and neural networks. Given the outstanding flexibility that Hopfield networks have recently been shown to have [84], it is easy to imagine how more general interaction matrices than the ones considered here can allow for other information processing tasks [85].

From the biology point of view, our work hints towards an analogy between the cellular cytoplasm and neural networks. Structured protein complexes are the cytoplasmic analogs of neuronal spatial maps [83,86,87], and biomolecular condensates are the cytoplasmic analogs of associative memories [11,31]. A promising next step guided by this analogy is investigating whether the evolution of the cytoplasm can be understood as a neural learning rule. Indeed, Refs. [24,26] demonstrate that point mutations are sufficient to change the phenomenology of protein phase separation, yielding aberrant condensates. This suggests that the interactions between proteins have been learned through evolutionary adaptation to optimize the formation of liquid phases. All in all, whether this "cytoplasm-neural network analogy" can be useful beyond a mathematical equivalence remains a stimulating direction for future inquiry.

ACKNOWLEDGMENTS

R. B. T. acknowledges financial support from the Portuguese Foundation for Science and Technology (FCT) under Contract No. 2022.12272.BD. This work was financially supported by core funding from GIMM to P. S. and D. M. The authors would like to thank G. Carugno for valuable contributions at the early stages of this work, T. E. Veenstra for feedback on Fig. 6, and T. Rotheray for proofreading the manuscript. We furthermore thank C. F. Lee for valuable discussions.

DATA AVAILABILITY

The data that support the findings of this article are not publicly available. The data are available from the authors upon reasonable request.

APPENDIX A: THERMODYNAMICS OF INCOMPRESSIBLE MULTICOMPONENT MIXTURES

We describe the thermodynamics of an incompressible mixture consisting of N solutes and a solvent. We consider the setup for which the temperature, volume, and molar numbers of the components are fixed. This setup is often considered in the literature, even though experiments typically are performed at constant pressure and real mixtures are not necessarily incompressible [3]. The advantage of this setup is that it is compatible with simple continuum models that are easily amenable to spatial simulations [1], such as the Flory-Huggins model and its variants [45,55,88].

The thermodynamic state parameters of the mixture in this setup are the temperature, T; the volume, V; the number of molecules of the solvent, M_0; and the number of molecules of the N solutes, M_i, with $i = 1, \ldots, N$. The corresponding thermodynamic potential for these $N+3$ variables is the Helmholtz free energy

$$F = F(T, V, M_0, \vec{M}), \tag{A1}$$

where $\vec{M} = (M_1, \ldots, M_N)$. Its differential expression is given by

$$\mathrm{d}F = -S\mathrm{d}T - p\mathrm{d}V + \sum_{i=0}^{N} \mu_i \mathrm{d}M_i, \tag{A2}$$

where S is the entropy, p the pressure, and μ_i are the chemical potentials. Differential forms for the latter quantities can also be expressed in terms of the state variables. For the pressure this gives

$$\mathrm{d}p = \left(\frac{\partial p}{\partial T}\right)_{V,\tilde{M}} \mathrm{d}T + \left(\frac{\partial p}{\partial V}\right)_{T,\tilde{M}} \mathrm{d}V + \sum_{i=0}^{N} \left(\frac{\partial p}{\partial M_i}\right)_{T,V,\tilde{M}'(i)} \mathrm{d}M_i, \tag{A3}$$

where $\tilde{M}$ denotes the vector $\tilde{M} = (M_0, \vec{M})$, and $\tilde{M}'(i)$ denotes all variables M_j for which $j \neq i$.

Incompressibility implies that the pressure can only be changed by varying the temperature, while changes in volume and composition result in divergent pressure. Mathematically, this is the limit for which

$$\left(\frac{\partial p}{\partial V}\right)_{T,\tilde{M}} \to \infty, \tag{A4}$$

$$\left(\frac{\partial p}{\partial T}\right)_{V,\tilde{M}} \left(\frac{\partial p}{\partial V}\right)^{-1}_{T,\tilde{M}} \to 0, \tag{A5}$$

$$\left(\frac{\partial p}{\partial M_i}\right)_{T,V,\tilde{M}'(i)} \left(\frac{\partial p}{\partial V}\right)^{-1}_{T,\tilde{M}} \to \text{constant}. \tag{A6}$$

These conditions can be rendered into a more intuitive form by using the chain rule. Indeed, the first condition states that the isothermal compressibility, $\kappa_T = -V^{-1}(\partial V/\partial p)_{T,\tilde{M}}$, is null; the second condition states that the thermal expansion coefficient, $\alpha = V^{-1}(\partial V/\partial T)_{p,\tilde{M}}$, is null; and the third condition states that the molecular volumes of all components, $\nu_i = (\partial V/\partial M_i)_{T,p,\tilde{M}'(i)}$, are constant (independent of state variables). From these conditions we can isolate the volume differential in Eq. (A3) as

$$\mathrm{d}V = \sum_{i=0}^{N} \nu_i \mathrm{d}M_i, \tag{A7}$$

which can be integrated to give

$$V = \sum_{i=0}^{N} \nu_i M_i. \tag{A8}$$

This equation is a constraint that allows us to remove one of the extensive thermodynamic parameters in the problem. We choose to remove M_0, without any loss of generality, and so the free energy of the incompressible system is

$$F = F_{\mathrm{inc}}(T, V, \vec{M}), \tag{A9}$$

where $F_{\mathrm{inc}}(T, V, \vec{M}) = F(T, V, M_0(V, \vec{M}), \vec{M})$ is the free energy in Eq. (1), and with $M_0(V, \vec{M})$ obtained from Eq. (A8). Hereafter, and in the main text, we drop the subindex "inc."

Next, we develop the intensive formulation of this incompressible setting. First, we note that the free energy density f is defined by

$$f(T, \rho_1, \ldots, \rho_N) = \frac{F(T, V, M_1, \ldots, M_N)}{V} = F(T, 1, \rho_1, \ldots, \rho_N). \tag{A10}$$

Here, $\rho_i = M_i/V$ are the number densities of the solutes. For the second equality of (A10) we have used that F is a homogeneous first-order function of its extensive parameters, which follows from the postulates of thermodynamics [16]. It is convenient to express densities in terms of volume fractions ϕ_i through

$$\phi_i = \rho_i \nu_i. \tag{A11}$$

The incompressibility constraint (A8) reduces to $\phi_0 = 1 - \sum_{i=1}^{N} \phi_i$, which implies $\sum_{i=1}^{N} \phi_i \leq 1$. Using Eq. (A11) and the fact that the ν_i are constants, we can define a free energy potential that is a function of volume fractions, viz.,

$$f_\phi(T, \phi_1, \ldots, \phi_N) = f(T, \phi_1/\nu_1, \ldots, \phi_N/\nu_N). \tag{A12}$$

The function f_ϕ is the free energy as it appears in (2), although in the main text we drop the ϕ subindex.

To finalize, we note that the exchange chemical potentials of the solutes can be written as

$$\bar{\mu}_i = \left(\frac{\partial F}{\partial M_i}\right)_{T,V,\vec{M}'(i)} = \nu_i \left(\frac{\partial f_\phi}{\partial \phi_i}\right)_{T,\vec{\phi}'(i)}, \quad \text{(A13)}$$

where M_0 and ϕ_0 are determined by the incompressibility constraints. The osmotic pressure can be written as

$$\Pi = -\left(\frac{\partial F}{\partial V}\right)_{T,\vec{M}} = -f + \sum_{i=1}^{N} \phi_i \left(\frac{\partial f_\phi}{\partial \phi_i}\right)_{T,\vec{\phi}'(i)}, \quad \text{(A14)}$$

where we have used that $F = Vf$ and $\phi_i = M_i \nu_i / V$, and as before M_0 is not fixed. The exchange chemical potentials and the osmotic pressure appear in the stationarity conditions for phase separation and thus play an important role in this paper. In fact, we note that due to incompressibility, the chemical potentials, $\mu_i = (\partial F/\partial M_i)_{T,V,\tilde{M}'(i)}$, are not well defined, as any change in the number of components of the system leads to a change in volume, thus violating incompressibility. The pressure, $p = -(\partial F/\partial V)_{T,\tilde{M}}$, is also not well defined, since any change in volume must be associated with change in the number of components, which is inconsistent with the thermodynamic definition of pressure.

APPENDIX B: CONSTRAINED PERTURBATION OF A PHASE SEPARATED STATE

To derive the stationarity and stability conditions of spatially heterogeneous states, we study how the free energy $\mathfrak{f}$ changes in response to a perturbation in the volume fractions and in the volume of the compartments. Therefore, considering the reference state $(\{w^{(c)}\}, \{\vec{\phi}^{(c)}\})$, we study the perturbed state characterized by $\tilde{w}^{(c)} = w^{(c)} + \epsilon^{(c)}$ and $\tilde{\phi}_i^{(c)} = \phi_i^{(c)} + \delta_i^{(c)}$, where $\epsilon^{(c)}$ and $\delta_i^{(c)}$ are the compartment volume and the compartment composition perturbation parameters. As the perturbed state must also be compatible with the constraints in Eqs. (8) and (9), we have that

$$\sum_{c=1}^{C} (w^{(c)} + \epsilon^{(c)}) = 1, \quad \text{(B1)}$$

and also

$$\phi_i = \sum_{c=1}^{C} (w^{(c)} + \epsilon^{(c)})(\phi_i^{(c)} + \delta_i^{(c)}). \quad \text{(B2)}$$

Using the constraint on the volumes of the reference state, Eq. (B1) returns

$$\epsilon^{(C)} = -\sum_{c<C} \epsilon^{(c)}. \quad \text{(B3)}$$

Additionally, using the volume and composition constraints of the reference state, we can write Eq. (B2) as

$$\sum_{c<C} (w^{(c)} + \epsilon^{(c)})\delta_i^{(c)} + \left(1 - \sum_{c<C} w^{(c)} + \epsilon^{(C)}\right)\delta_i^{(C)} = -\Gamma_i, \quad \text{(B4)}$$

with $\Gamma_i = \sum_{c<C} \epsilon^{(c)}(\phi_i^{(c)} - \phi_i^{(C)})$. These two latter equations constitute constraints on the perturbation parameters. In particular, expanding Eq. (B4) to quadratic order we obtain

$$\delta_i^{(C)} = -\sum_{c<C} \delta_i^{(c)} \frac{w^{(c)}}{1 - \sum_{c<C} w^{(c)}} + \sum_{c<C} \epsilon^{(c)} \frac{(\phi_i^{(C)} - \phi_i^{(c)})}{1 - \sum_{c<C} w^{(c)}} + O(\epsilon\delta, \delta^2, \epsilon^2). \quad \text{(B5)}$$

We now move on to evaluate the free energy of the perturbed state, $\tilde{\mathfrak{f}} = \mathfrak{f}(\{\tilde{w}^{(c)}\}, \{\tilde{\vec{\phi}}^{(c)}\})$. Expanding to second order and using Eq. (B4) to express the term $(1 - \sum w^{(c)} - \sum \epsilon^{(c)}) \sum_{i=1}^{N} \delta_i^{(C)} \partial_i f^{(C)}$ in terms of Γ_i and $\delta_i^{(c)}$, the free energy of the perturbed state can be written as

$$\begin{aligned}\tilde{\mathfrak{f}} = \mathfrak{f} &+ \sum_{c<C} \epsilon^{(c)} \left[f(\vec{\phi}^{(c)}) - f(\vec{\phi}^{(C)}) - \sum_i (\phi_i^{(c)} - \phi_i^{(C)}) \partial_i f^{(c)} \right] \\ &+ \sum_{c<C} \sum_i \delta_i^{(c)} [w^{(c)} (\partial_i f^{(c)} - \partial_i f^{(C)})] \\ &+ \sum_{c<C} w^{(c)} \frac{1}{2} \sum_{ij} \delta_i^{(c)} \delta_j^{(c)} h_{ij}^{(c)} \\ &+ \left(1 - \sum_{c<C} w^{(c)}\right) \frac{1}{2} \sum_{ij} \delta_i^{(C)} \delta_j^{(C)} h_{ij}^{(C)} \\ &- \sum_i \sum_{c<C} \epsilon^{(c)} \delta_i^{(c)} (\partial_i f^{(C)} - \partial_i f^{(c)}). \end{aligned} \quad \text{(B6)}$$

In the following sections, we study the first and second order terms of this perturbation to establish the stationarity and stability conditions of a phase separated state.

APPENDIX C: STATIONARITY CONDITIONS OF PHASE SEPARATED STATES

To obtain the stationarity conditions we set the first order terms in the perturbative expansion (B6) to zero. Since the perturbation variables themselves, $\epsilon^{(c)}$ and $\delta_i^{(c)}$, are arbitrary, the factors in the brackets must be null. Setting to zero the factor in the second term yields

$$\partial_i f^{(c)} = \partial_i f^{(C)} \quad \text{(C1)}$$

for any i and any c. Using the definition of exchange chemical potential, Eq. (3), we obtain the chemical balance condition in Eq. (10). Similarly, the factor in the brackets of the first term is null if and only if

$$f^{(c)} - \sum_i \partial_i f^{(c)} \phi_i^{(c)} = f^{(C)} - \sum_i \partial_i f^{(C)} \phi_i^{(C)}, \tag{C2}$$

where we have used the condition of chemical balance. Using the expression of osmotic pressure we thus derive the conditions of mechanical balance in Eq. (11).

The compositions of the phases define a plane that passes through all P points $(\vec{\phi}^{(c)}, f^{(c)})$ and is tangent to the free energy surface $f(\vec{\phi})$. To see this, first note that the equation for a tangent plane that passes through a point $(\vec{\phi}^{(c)}, f^{(c)})$ in $\mathbb{R}^{N+1}$ is given by

$$z = f^{(c)} + \sum_i \partial_i f^{(c)} (\varphi_i - \phi_i^{(c)}), \tag{C3}$$

where $(z, \vec{\varphi}) \in \mathbb{R}^{N+1}$. This can also be written as

$$z = f^{(c)} - \sum_i \partial_i f^{(c)} \phi_i^{(c)} + \sum_i \partial_i f^{(c)} \varphi_i. \tag{C4}$$

Because of Eq. (C1), the last term in the right-hand side of the expression above is the same for all c; and due to Eq. (C2) the first two terms are also the same for all c. Therefore, the set of P composition vectors that satisfies the stationarity conditions define a common tangent plane. In addition, since $\vec{\phi} = \sum_{c=1}^{P} w^{(c)} \vec{\phi}^{(c)}$, we find that the compositions are restricted to a simplex within that plane.

APPENDIX D: STABILITY CONDITIONS

The stability conditions of phase separated states are obtained by imposing that any small change in free energy at a given stationary point is positive. We therefore evaluate the change in free energy $\Delta \mathfrak{f} = \tilde{\mathfrak{f}} - \mathfrak{f}$. Stationarity implies that the linear terms and the cross-quadratic terms vanish, and so we have

$$\Delta \mathfrak{f} = \sum_{c=1}^{C} w^{(c)} \frac{1}{2} \sum_{ij} \delta_i^{(c)} \delta_j^{(c)} h_{ij}^{(c)}, \tag{D1}$$

where the volume in the last compartment is given by Eq. (8) and the corresponding perturbation in composition by Eq. (B5). From the expression (D1), we find that if the Hessians of all compartments are positive definite, then the change in free energy must be positive, and the state is stable. Therefore, stability of all phases composing phase separated states is sufficient for stability of the phase separated state.

To prove the converse, i.e., that stability of all phases is necessary for the stability of the phase separated state, we show that if one phase is unstable, then there always exists a perturbation that lowers the free energy of the phase separated state. Thus, consider a system with P phases, with one of them being unstable. We represent the system by $C = P + 1$ compartments, with the compartments $c = 1$ and $c = 2$ representing the same phase, which is the unstable one. We also set the compartment volumes in these two compartments equal to each other. In this setup, we study the following perturbation

$$\vec{\delta}^{(c)} = (\delta_{c,1} - \delta_{c,2}) \vec{r}, \tag{D2}$$

with $\vec{r}$ the component perturbation vector. The perturbation $\vec{\delta}^{(c)}$ only affects the first two compartments, and leaves the remaining ones intact. Furthermore, the fact that $\delta_i^{(1)} = -\delta_i^{(2)} = r_i$ ensures that the constraint in Eq. (B5) is satisfied. For this perturbation, the change in free energy from Eq. (13) takes the form

$$\Delta \mathfrak{f} = w^{(1)} \sum_{ij} h_{ij}^{(1)} r_i r_j, \tag{D3}$$

and so it follows that if the Hessian of the phase has negative eigenvalues, a reduction in free energy of the phase separated states is possible. Thus, we conclude that stability of all phases is necessary (and also sufficient) for stability of the phase separated state.

We finalize by showing how to write the change in free energy of a phase separated phase as a quadratic form. To do so, we use Eq. (B5) in Eq. (D1), which gives

$$\begin{aligned}
\Delta \mathfrak{f} = {} & \frac{1}{2} \sum_{ij} \sum_{c<C} \delta_i^{(c)} \delta_j^{(c)} w^{(c)} h_{ij}^{(c)} \\
& + \frac{1}{2w^{(C)}} \sum_{ij} \sum_{c<C} \delta_i^{(c)} w^{(c)} h_{ij}^{(C)} \sum_{d<C} \delta_j^{(d)} w^{(d)} \\
& + \frac{1}{2w^{(C)}} \sum_{ij} \sum_{c<C} \epsilon^{(c)} \Delta_i^{(c)} h_{ij}^{(C)} \sum_{d<C} \epsilon^{(d)} \Delta_j^{(d)} \\
& - \frac{1}{2w^{(C)}} \sum_{ij} \sum_{c<C} \delta_i^{(c)} w^{(c)} h_{ij}^{(C)} \sum_{d<C} \epsilon^{(d)} \Delta_j^{(d)} \\
& - \frac{1}{2w^{(C)}} \sum_{ij} \sum_{c<C} \delta_j^{(c)} w^{(c)} h_{ij}^{(C)} \sum_{d<C} \epsilon^{(d)} \Delta_i^{(d)},
\end{aligned} \tag{D4}$$

and where we have defined $\Delta_i^{(c)} = (\phi_i^{(C)} - \phi_i^{(c)})$. We can thus write $\Delta \mathfrak{f}$ in terms of a matrix $\mathbf{A}$ which has the block form

$$\mathbf{A} = \begin{pmatrix} \mathbf{P} & \mathbf{Q} \\ \mathbf{Q}^\top & \mathbf{R} \end{pmatrix}. \tag{D5}$$

Here, the matrix $\mathbf{R}$ is a square matrix of size $C - 1$ and with elements

$$R_{cd} = \frac{1}{w^{(C)}} (\vec{\Delta}^{(c)})^{\top} \cdot \mathbf{h}^{(C)} \cdot \vec{\Delta}^{(d)}. \tag{D6}$$

The matrix $\mathbf{Q}$ is a rectangular matrix with dimensions $(C-1)N \times (C-1)$. It can be defined through $(C-1)^2$ blocks, each corresponding to a vector of size N:

$$\vec{Q}_{cd} = -\frac{w^{(c)}}{w^{(C)}} \mathbf{h}^{(C)} \cdot \vec{\Delta}^{(d)}. \tag{D7}$$

Finally, the matrix $\mathbf{P}$ is square, and has size $N(C-1)$. It can be defined through $(C-1)^2$ blocks each corresponding to a square matrix of size N:

$$P_{cd} = \delta_{cd} w^{(c)} \mathbf{h}^{(c)} + \frac{w^{(c)} w^{(d)}}{w^{(C)}} \mathbf{h}^{(C)}. \tag{D8}$$

This completes the definition of $\mathbf{A}$.

We note that stationarity and stability conditions of phase separated states of multicomponent mixtures can also be derived with an alternative, algebraic approach that uses Lagrange multipliers and the bordered Hessian. The interested reader can find this algebraic method in Supplemental Material Sec. S3 [32].

APPENDIX E: PHASE SEPARATION DYNAMICS

In this section we provide a minimal framework to describe the spatiotemporal dynamics of phase separation of incompressible mixtures based on linearly irreversible thermodynamics [89]. This approach, which is a straightforward generalization of Cahn-Hilliard dynamics [46,55], generalizes the thermodynamic variables of multicomponent mixtures to continuous spatial fields (locally at equilibrium) that can vary over time, taking into account the role of interfacial energy.

Consider the position vector $\boldsymbol{r}$ spanning the whole volume V of the vessel that contains the mixture (hereafter we use bold font to denote quantities that are spatial vectors). Symbolically, this can be expressed as $\int_V \mathrm{d}\boldsymbol{r} = V$, which is analogous to Eq. (8). We aim at characterizing the time evolution of the solute composition fields $\phi_i(\boldsymbol{r}, t)$, with $i = 1, \ldots, N$ [as in the main text, we will use arrows to denote vectors in composition space, e.g. $\vec{\phi}(\boldsymbol{r}, t)$]. The total abundances of components are conserved, and so

$$\frac{1}{V} \int_V \phi_i(\boldsymbol{r}, t) \mathrm{d}\boldsymbol{r} = \phi_i, \tag{E1}$$

which generalizes Eq. (9), and shows that ϕ_i is dimensionless. To enforce these constraints, the composition fields follow the conservation equation

$$\frac{\partial \phi_i(\boldsymbol{r}, t)}{\partial t} = -\nabla \cdot \boldsymbol{J}_i(\boldsymbol{r}, t), \tag{E2}$$

where the vector field $\boldsymbol{J}_i$ is the volume flux of species i, and has units of volume per unit area and time, i.e., length per time.

Following the standard formalism of linearly irreversible thermodynamics [89], we take that these fluxes are linear in the gradients of the corresponding driving forces. The driving forces corresponding to the density fields are their thermodynamic conjugate variables, the exchange chemical potential fields $\bar{\mu}(\boldsymbol{r}, t)$, which have units of energy density. We thus have

$$\boldsymbol{J}_i(\boldsymbol{r}, t) = -\sum_{j=1}^{N} L_{ij} \nabla \bar{\mu}_j(\boldsymbol{r}, t), \tag{E3}$$

where the transport matrix L_{ij} is symmetric, which is a formulation of Onsager's relations (L_{ij} has units of area per energy and time). To determine the exchange chemical potential fields, we define the free energy functional $\mathfrak{F} = \mathfrak{F}[\vec{\phi}(\boldsymbol{r}, t)]$ as

$$\mathfrak{F}[\vec{\phi}(\boldsymbol{r}, t)] = \int_V f(\vec{\phi}(\boldsymbol{r}, t), \nabla \vec{\phi}(\boldsymbol{r}, t)) \mathrm{d}\boldsymbol{r}, \tag{E4}$$

where the free energy density $f(\vec{\phi}, \nabla\vec{\phi})$ includes a gradient dependence to account for interfacial tension, and thus generalizes the homogeneous free energy density in the main text. The exchange chemical potential fields are then given by the functional derivatives of $\mathfrak{F}[\vec{\phi}(\boldsymbol{r}, t)]$ with respect to the composition fields, i.e.,

$$\bar{\mu}_i(\boldsymbol{r}, t) = \nu_i \frac{\delta \mathfrak{F}[\vec{\phi}(\boldsymbol{r}, t)]}{\delta \phi_i(\boldsymbol{r}, t)}. \tag{E5}$$

We take as free energy density functional a simple generalization of Cahn-Hilliard expression to multicomponent mixtures [46,55]. In this case, we have

$$f(\vec{\phi}, \nabla\vec{\phi}) = f(\vec{\phi}) + \sum_{i=1}^{N} \sum_{j=1}^{N} \frac{K_{ij}}{2} (\nabla \phi_i) \cdot (\nabla \phi_j). \tag{E6}$$

Here $f(\vec{\phi})$ is the homogeneous free energy density of the main text, and the second term characterizes the free energy of the interface between domains with different composition, with the symmetric matrix K_{ij} determining the energetic cost for gradients of different solutes [2], and measured in units of energy per unit length.

The equations above provide a closed dynamical system, which captures the dynamics of phase separation. To fully complete the system there are multiple model parameters that need to be provided: the total volume fractions $\vec{\phi}$, the interaction tensors, and the matrices of transport and interfacial energy. In this work, we exclusively focus on the particular case in which $L_{ij} = \ell \delta_{ij}$ and $K_{ij} = k\delta_{ij}$,

where the parameter ℓ sets the timescale of transport and k the spatial scale of interfaces; see Supplemental Material Sec. S6 [32] for a discussion of units. With spatially uniform ℓ, k, the exchange chemical potentials and fluxes read

$$\bar{\mu}_i(\boldsymbol{r},t) = \nu_i\left[\frac{\partial f}{\partial \phi_i}(\vec{\phi}) - k\nabla^2\phi_i\right], \tag{E7}$$

$$\boldsymbol{J}_i(\boldsymbol{r},t) = -\ell\nabla\bar{\mu}_i(\boldsymbol{r},t). \tag{E8}$$

Inserting these into the continuity equation yields the multicomponent Cahn-Hilliard system of equations

$$\frac{\partial\phi_i}{\partial t} = \ell\nu_i\nabla^2\left[\frac{\partial f}{\partial\phi_i}(\vec{\phi}) - k\nabla^2\phi_i\right], \quad i = 1,\ldots,N. \tag{E9}$$

A nondimensional version of this equation can be found in Supplemental Material Sec. S6 [32].

APPENDIX F: STATIONARITY CONDITIONS FOR PHASE SEPARATED STATES IN THE LIQUID HOPFIELD MODEL

We derive the conditions for stationarity of a phase separated state that corresponds to a target and its complement, i.e., $C = 2$ (see also Supplemental Material Sec. S8 and S9 [32] for details on calculations). Here, we generalize the results in the main text for the case of arbitrary q, and so the ansatz for the compositions is

$$\phi_i^{(\alpha)} = \frac{\phi_+}{N}\left(1 + a_+\gamma_i^{(\alpha)}\right), \tag{F1}$$

$$\phi_i^{(-\alpha)} = \frac{\phi_-}{N}\left(1 - a_-\gamma_i^{(\alpha)}\right), \tag{F2}$$

where $\phi_+ = \sum_i \phi_i^{(\alpha)}$ and $\phi_- = \sum_i \phi_i^{(-\alpha)}$ are the total densities of the retrieval phase and the antiretrieval phase, and $a_+ = \sum_i \phi_i^{(\alpha)}\gamma_i^{(\alpha)}/\phi_+$ and $a_- = -\sum_i \phi_i^{(-\alpha)}\gamma_i^{(\alpha)}/\phi_-$ are the overlap parameters that quantify the enrichment and depletion of components in these compartments in accordance to the given target. For the volume of the compartments we have that $w^{(\alpha)} = 1 - w^{(-\alpha)}$, and simplify notation by writing $w^{(\alpha)} = w$. Therefore, in order to obtain a stationary solution we need to determine five parameters: w, a_+, a_-, ϕ_+, and ϕ_-.

We start by considering the density constraints from Eq. (9). Using the expressions in Eq. (F1) we obtain that the N constraints reduce to two different constraints, one for components in which $\xi_i^{(\alpha)} = 1$ and another for components in which $\xi_i^{(\alpha)} = 0$. After some manipulations, the two constraints can be written as

$$\phi_+ = \frac{\phi}{w}\frac{a_-}{a_+ + a_-}, \tag{F3}$$

$$\phi_- = \frac{\phi}{1-w}\frac{a_+}{a_+ + a_-}. \tag{F4}$$

These two equations allow us to compute ϕ_+ and ϕ_- from the remaining three parameters.

Next, we consider the conditions of chemical balance from Eq. (10). In each compartment the components have two possible values for the exchange chemical potential, depending on whether they are present or absent in the retrieval phase. Therefore, chemical balance provides two different equations: $\mu_i^{(\alpha)} = \mu_i^{(-\alpha)}$ for $\xi_i^\alpha = 1$, and $\mu_i^{(\alpha)} = \mu_i^{(-\alpha)}$ for $\xi_i^\alpha = 0$. Writing these two equations and further using Eq. (F1) results in two equations with three unknowns, a_+, a_-, and w. After some algebra, these two equations can be written as

$$a_+ = n\frac{(1-w)(e^f - e^g)}{(1-w)[(1-q)e^g + e^f q] + we^{f+g}}, \tag{F5}$$

$$a_- = n\frac{w(e^f - e^g)}{1 - w + w[(1-q)e^f + qe^g]}, \tag{F6}$$

where the functions f and g are given by

$$\begin{aligned} f(a_+,a_-,w) = {} & v_2\phi\frac{a_-a_+}{a_- + a_+}\left(\frac{1}{w(1-w)}\right)\left(\frac{1-q}{n} - \phi\frac{a_-a_+}{2(a_- + a_+)}\frac{1-2w}{(1-w)w}\right) \\ & - \frac{v_3\phi^2}{2(a_- + a_+)^2}\left(\frac{a_-^2}{w^2}(1 + a_+[1-q]/n)^2 - \frac{a_+^2}{(1-w)^2}(1 - a_-[1-q]/n)^2\right) \\ & + \frac{v_3\phi^3}{3(a_- + a_+)^3}\left(\frac{a_-^3}{w^3}\left(1 + 3a_+^2 + a_+^3\frac{1-2q}{n}\right) - \frac{a_+^3}{(1-w)^3}\left(1 + 3a_-^2 - a_-^3\frac{1-2q}{n}\right)\right), \end{aligned} \tag{F7}$$

$$g(a_+,a_-,w) = v_2\phi\frac{a_-a_+}{a_-+a_+}\left(\frac{1}{w(1-w)}\right)\left(-\frac{q}{n}-\phi\frac{a_-a_+}{2(a_-+a_+)}\frac{1-2w}{(1-w)w}\right) - \frac{v_3\phi^2}{2(a_-+a_+)^2}\left(\frac{a_-^2}{w^2}(1-a_+q/n)^2-\frac{a_+^2}{(1-w)^2}(1+a_-q/n)^2\right) + \frac{v_3\phi^3}{3(a_-+a_+)^3}\left(\frac{a_-^3}{w^3}\left(1+3a_+^2+a_+^3\frac{1-2q}{n}\right)-\frac{a_+^3}{(1-w)^3}\left(1+3a_-^2-a_-^3\frac{1-2q}{n}\right)\right). \tag{F8}$$

Lastly, we consider the balance of osmotic pressures across the two compartments. This constitutes a single equation that, after some manipulations, can be written as

$$-\frac{v_2\phi^2(a_-a_+)^2}{2(a_++a_-)^2}\left(\frac{1-2w}{(1-w)^2w^2}\right)+\frac{v_3\phi^3}{3(a_-+a_+)^3}\left(\frac{a_-^3}{w^3}\left(1+3a_+^2+a_+^3\frac{1-2q}{n}\right)-\frac{a_+^3}{(1-w)^3}\left(1+3a_-^2-a_-^3\frac{1-2q}{n}\right)\right) = \log\left(\frac{1-w}{w}\frac{w(a_++a_-)-\phi a_-}{(1-w)(a_++a_-)-\phi a_+}\right). \tag{F9}$$

Overall, Eqs. (F3), (F4), (F5), (F6), and (F9) constitute a system of five equations with five unknowns: ϕ_+, ϕ_-, a_+, a_-, and w. Solving this system towards the unknowns ensures that the phase separated state is stationary. We remark that this system of equations, which is valid for arbitrary values of q, reduces to the one in the main text for $q = 1/2$, as shown in Supplemental Material Sec. S8 [32].

APPENDIX G: STABILITY CONDITIONS FOR PHASE SEPARATED RETRIEVAL PHASES IN THE LIQUID HOPFIELD MODEL

Reference [11] derives sufficient conditions for the stability of stationary phases of the form (F1). These conditions are given in terms of the coefficients

$$c_1^{(\pm\alpha)} = v_3\phi_\pm(1\mp a_\pm q/n)+\frac{1}{\phi_\pm}\frac{1}{1\mp a_\pm q/n}, \tag{G1}$$

$$c_2^{(\pm\alpha)} = \mp\frac{v_3\phi_\pm a_\pm}{n} \pm\frac{a_\pm}{n\phi_\pm}\frac{1}{(1\pm a_\pm(1-q)/n)(1\mp a_\pm q/n)}, \tag{G2}$$

for the retrieval phase ($+\alpha$) and the anti-retrieval phase $-\alpha$. The conditions for stability take the form

$$-v_2+c_1^{(\pm\alpha)}-c_2^{(\pm\alpha)}>0 \quad \text{if } c_2^{(\pm\alpha)}\geq 0 \tag{G3}$$

$$-v_2+c_1^{(\pm\alpha)}>0 \quad \text{if } c_2^{(\pm\alpha)}<0. \tag{G4}$$

Note that a phase separated state consists of pairs of retrieval, anti-retrieval phases, and both phases must satisfy the Eqs. (G3) and (G4).

[1] M. Rubinstein and R. H. Colby, *Polymer Physics* (Oxford University Press, New York, 2003).
[2] S. Safran, *Statistical Thermodynamics of Surfaces, Interfaces, and Membranes* (CRC Press, Boca Raton, 2003).
[3] P. W. Atkins and J. De Paula, *Atkins' Physical Chemistry*, 8th ed. (W. H. Freeman and Company, New York, 2006).
[4] L. V. Schaffer, M. Hu, G. Qian, K.-M. Moon, A. Pal, N. Soni, A. P. Latham, L. Pontano Vaites, D. Tsai, N. M. Mattson *et al.*, *Multimodal cell maps as a foundation for structural and functional genomics*, Nature (London) **642**, 222 (2025).
[5] S. F. Banani, H. O. Lee, A. A. Hyman, and M. K. Rosen, *Biomolecular condensates: Organizers of cellular biochemistry*, Nat. Rev. Mol. Cell Biol. **18**, 285 (2017).
[6] B. R. Sabari, A. Dall'Agnese, and R. A. Young, *Biomolecular condensates in the nucleus*, Trends Biochem. Sci. **45**, 961 (2020).
[7] K. You, Q. Huang, C. Yu, B. Shen, C. Sevilla, M. Shi, H. Hermjakob, Y. Chen, and T. Li, *Phasepdb: A database of liquid–liquid phase separation related proteins*, Nucl. Acids Res. **48**, D354 (2020).
[8] Y. Wang and L.-L. Chen, *Organization and function of paraspeckles*, Essays Biochem. **64**, 875 (2020).
[9] J. S. Andersen, C. E. Lyon, A. H. Fox, A. K. Leung, Y. W. Lam, H. Steen, M. Mann, and A. I. Lamond, *Directed proteomic analysis of the human nucleolus*, Curr. Biol. **12**, 1 (2002).
[10] M. Machyna, P. Heyn, and K. M. Neugebauer, *Cajal bodies: Where form meets function*, Wiley Interdiscip. Rev. **4**, 17 (2013).
[11] R. Braz Teixeira, G. Carugno, I. Neri, and P. Sartori, *Liquid hopfield model: Retrieval and localization in multicomponent liquid mixtures*, Proc. Natl. Acad. Sci. U.S.A. **121**, e2320504121 (2024).
[12] R. P. Sear and J. A. Cuesta, *Instabilities in complex mixtures with a large number of components*, Phys. Rev. Lett. **91**, 245701 (2003).

[13] W. M. Jacobs and D. Frenkel, *Predicting phase behavior in multicomponent mixtures*, J. Chem. Phys. **139**, 024108 (2013).
[14] F. C. Thewes, M. Krüger, and P. Sollich, *Composition dependent instabilities in mixtures with many components*, Phys. Rev. Lett. **131**, 058401 (2023).
[15] D. Zwicker and L. Laan, *Evolved interactions stabilize many coexisting phases in multicomponent liquids*, Proc. Natl. Acad. Sci. U.S.A. **119**, e2201250119 (2022).
[16] H. B. Callen, *Thermodynamics and an introduction to thermostatistics*, 2nd ed. (Wiley, New York, 1985).
[17] H. Frauenfelder, S. G. Sligar, and P. G. Wolynes, *The energy landscapes and motions of proteins*, Science **254**, 1598 (1991).
[18] J. N. Onuchic, Z. Luthey-Schulten, and P. G. Wolynes, *Theory of protein folding: The energy landscape perspective*, Annu. Rev. Phys. Chem. **48**, 545 (1997).
[19] M. Mézard, G. Parisi, and M. A. Virasoro, *Spin Glass Theory and Beyond: An Introduction to the Replica Method and Its Applications* (World Scientific Publishing Company, Singapore, 1987), Vol. 9.
[20] P. Charbonneau, E. Marinari, G. Parisi, F. Ricci-tersenghi, G. Sicuro, F. Zamponi, and M. Mezard, *Spin Glass Theory and Far Beyond: Replica Symmetry Breaking after 40 Years* (World Scientific, Singapore, 2023).
[21] H. M. Jaeger, S. R. Nagel, and R. P. Behringer, *Granular solids, liquids, and gases*, Rev. Mod. Phys. **68**, 1259 (1996).
[22] J. Hertz, A. Krogh, and R. G. Palmer, *Introduction to the Theory of Neural Computation* (CRC Press, Boca Raton, 2018).
[23] Y. Qiang, C. Luo, and D. Zwicker, *Generic multicomponent mixtures are multistable*, arXiv:2405.01138.
[24] A. Patel, H. O. Lee, L. Jawerth, S. Maharana, M. Jahnel, M. Y. Hein, S. Stoynov, J. Mahamid, S. Saha, T. M. Franzmann *et al.*, *A liquid-to-solid phase transition of the ALS protein FUS accelerated by disease mutation*, Cell **162**, 1066 (2015).
[25] Y. Lin, D. S. Protter, M. K. Rosen, and R. Parker, *Formation and maturation of phase-separated liquid droplets by RNA-binding proteins*, Mol. Cell **60**, 208 (2015).
[26] T. Das, F. K. Zaidi, M. Farag, K. M. Ruff, T. S. Mahendran, A. Singh, X. Gui, J. Messing, J. P. Taylor, P. R. Banerjee *et al.*, *Tunable metastability of condensates reconciles their dual roles in amyloid fibril formation*, Mol. Cell **85**, 2230 (2025).
[27] T. C. Michaels, D. Qian, A. Šarić, M. Vendruscolo, S. Linse, and T. P. Knowles, *Amyloid formation as a protein phase transition*, Nat. Rev. Phys. **5**, 379 (2023).
[28] Y. Du, C. Chalk, S. Buse, L. Qian, and E. Winfree, *Contrastive Hebbian learning for multicomponent liquids*, in *32nd International Conference on DNA Computing and Molecular Programming (DNA 32), LIPIcs, Vol. 387*, (Schloss Dagstuhl, Dagstuhl, 2026), p. 13:1.
[29] S.-I. Amari, *Learning patterns and pattern sequences by self-organizing nets of threshold elements*, IEEE Trans. Comput. **100**, 1197 (1972).
[30] L. A. Pastur and A. L. Figotin, *Exactly soluble model of a spin glass*, Sov. J. Low Temp. Phys. **3**, 378 (1977).
[31] J. J. Hopfield, *Neural networks and physical systems with emergent collective computational abilities.*, Proc. Natl. Acad. Sci. U.S.A. **79**, 2554 (1982).
[32] See Supplemental Material at http://link.aps.org/supplemental/10.1103/lxrw-98f4 for details regarding analytical derivations and the numerical implementation of the Cahn-Hilliard simulations, as well as for additional figures. The Supplemental Material includes Refs. [33–37].
[33] O. Adame-Arana, C. A. Weber, V. Zaburdaev, J. Prost, and F. Jülicher, *Liquid phase separation controlled by pH*, Biophys. J. **119**, 1590 (2020).
[34] S. J. Colley, *Vector Calculus*, 4th ed. (Pearson Education, Inc., 2012).
[35] L. Q. Chen and J. Shen, *Applications of semi-implicit Fourier-spectral method to phase field equations*, Comput. Phys. Commun. **108**, 147 (1998).
[36] V. A. Marčenko and L. A. Pastur, *Distribution of eigenvalues for some sets of random matrices*, Math. USSR-Sbor. **1**, 457 (1967).
[37] R. E. Paley, *On orthogonal matrices*, J. Math. Phys. (N.Y.) **12**, 311 (1933).
[38] E. Fermi, *Thermodynamics* (Courier Corporation, New York, 2012).
[39] D. Zwicker, O. W. Paulin, and C. ter Burg, *Physics of droplet regulation in biological cells*, arXiv:2501.13639.
[40] D. Zwicker, *The intertwined physics of active chemical reactions and phase separation*, Curr. Opin. Colloid Interface Sci. **61**, 101606 (2022).
[41] J. W. Cahn, *The metastable liquidus and its effect on the crystallization of glass*, J. Am. Ceram. Soc. **52**, 118 (1969).
[42] R. Evans, W. Poon, and M. Cates, *Role of metastable states in phase ordering dynamics*, Europhys. Lett. **38**, 595 (1997).
[43] R. M. L. Evans and M. E. Cates, *Diffusive evolution of stable and metastable phases. i. Local dynamics of interfaces*, Phys. Rev. E **56**, 5738 (1997).
[44] P. D. Olmsted, W. C. K. Poon, T. C. B. McLeish, N. J. Terrill, and A. J. Ryan, *Spinodal-assisted crystallization in polymer melts*, Phys. Rev. Lett. **81**, 373 (1998).
[45] P. J. Flory, *Thermodynamics of high polymer solutions*, J. Chem. Phys. **10**, 51 (1942).
[46] J. W. Cahn and J. E. Hilliard, *Free energy of a nonuniform system. i. Interfacial free energy*, J. Chem. Phys. **28**, 258 (1958).
[47] S. Z. Cheng, *Phase Transitions in Polymers: The Role of Metastable States* (Elsevier, New York, 2008).
[48] C. Chalk, S. Buse, K. Shrinivas, A. Murugan, and E. Winfree, *Learning and inference in a lattice model of multicomponent condensates* (2024).
[49] A. S. Chaderjian, S. Wilken, and O. A. Saleh, *Diverse, distinct, and densely packed DNA droplets*, Proc. Natl. Acad. Sci. U.S.A. **123**, e2523462123 (2026).
[50] G. Carugno, *Phase separation and instabilities of complex fluids*, Ph.D. thesis, 2023.
[51] E. H. Moore, *On the reciprocal of the general algebraic matrix*, Bull. Am. Math. Soc. **26**, 394 (1920).
[52] R. Penrose, *A generalized inverse for matrices*, Math. Proc. Cambridge Philos. Soc. **51**, 406 (1955).
[53] T. Kohonen, *Correlation matrix memories*, IEEE Trans. Comput. **100**, 353 (1972).
[54] V. Dotsenko, N. Yarunin, and E. Dorotheyev, *Statistical mechanics of hopfield-like neural networks with modified interactions*, J. Phys. A **24**, 2419 (1991).

[55] S. Mao, D. Kuldinow, M. P. Haataja, and A. Košmrlj, *Phase behavior and morphology of multicomponent liquid mixtures*, Soft Matter **15**, 1297 (2019).
[56] K. Shrinivas and M. P. Brenner, *Phase separation in fluids with many interacting components*, Proc. Natl. Acad. Sci. U.S.A. **118**, e2108551118 (2021).
[57] D. J. Amit, H. Gutfreund, and H. Sompolinsky, *Storing infinite numbers of patterns in a spin-glass model of neural networks*, Phys. Rev. Lett. **55**, 1530 (1985).
[58] G. Carugno, I. Neri, and P. Vivo, *Instabilities of complex fluids with partially structured and partially random interactions*, Phys. Biol. **19**, 056001 (2022).
[59] L. Parkavousi, N. Rana, R. Golestanian, and S. Saha, *Enhanced stability and chaotic condensates in multispecies nonreciprocal mixtures*, Phys. Rev. Lett. **134**, 148301 (2025).
[60] L. Parkavousi and S. Saha, *Compositional disorder in a multicomponent non-reciprocal mixture: Stability and patterns*, Phys. Rev. Res. **8**, 023223 (2025).
[61] W. M. Jacobs and D. Frenkel, *Phase transitions in biological systems with many components*, Biophys. J. **112**, 683 (2017).
[62] M. Girard, *On kinetics and extreme values in systems with random interactions*, Phys. Biol. **20**, 016006 (2022).
[63] F. Chen and W. M. Jacobs, *Programmable phase behavior in fluids with designable interactions*, J. Chem. Phys. 158 (2023).
[64] A.-C. Gavin, M. Bösche, R. Krause, P. Grandi, M. Marzioch, A. Bauer, J. Schultz, J. M. Rick, A.-M. Michon, C.-M. Cruciat *et al.*, *Functional organization of the yeast proteome by systematic analysis of protein complexes*, Nature (London) **415**, 141 (2002).
[65] K. L. Saar, R. M. Scrutton, K. Bloznelyte, A. S. Morgunov, L. L. Good, A. A. Lee, S. A. Teichmann, and T. P. Knowles, *Protein condensate atlas from predictive models of heteromolecular condensate composition*, Nat. Commun. **15**, 5418 (2024).
[66] Y. Sato, T. Sakamoto, and M. Takinoue, *Sequence-based engineering of dynamic functions of micrometer-sized dna droplets*, Sci. Adv. **6**, eaba3471 (2020).
[67] S. Biffi, R. Cerbino, F. Bomboi, E. M. Paraboschi, R. Asselta, F. Sciortino, and T. Bellini, *Phase behavior and critical activated dynamics of limited-valence dna nanostars*, Proc. Natl. Acad. Sci. U.S.A. **110**, 15633 (2013).
[68] C. Luo, Y. Qiang, and D. Zwicker, *Beyond pairwise: Higher-order physical interactions affect phase separation in multicomponent liquids*, Phys. Rev. Res. **6**, 033002 (2024).
[69] D. Zwicker, A. A. Hyman, and F. Jülicher, *Suppression of Ostwald ripening in active emulsions*, Phys. Rev. E **92**, 012317 (2015).
[70] J. Kirschbaum and D. Zwicker, *Controlling biomolecular condensates via chemical reactions*, J. R. Soc. Interface **18**, 20210255 (2021).
[71] A. Klosin, F. Oltsch, T. Harmon, A. Honigmann, F. Jülicher, A. A. Hyman, and C. Zechner, *Phase separation provides a mechanism to reduce noise in cells*, Science **367**, 464 (2020).
[72] J. Fries, R. Berthin, C. Luo, M. Jardat, D. Zwicker, V. Dahirel, and P. Illien, *Chemically active droplets in crowded environments*, J. Chem. Phys. **65**, 2013 (1976).
[73] F. Benoist and P. Sartori, *High-speed combinatorial polymerization through kinetic-trap encoding*, Phys. Rev. Lett. **134**, 038402 (2025).
[74] F. Benoist and P. Sartori, *Assembly factors resolve speed and encoding bottlenecks in multifarious self-assembly*, PRX Life **4**, 033021 (2026).
[75] S. Mao, M. S. Chakraverti-Wuerthwein, H. Gaudio, and A. Košmrlj, *Designing the morphology of separated phases in multicomponent liquid mixtures*, Phys. Rev. Lett. **125**, 218003 (2020).
[76] W. M. Jacobs, *Self-assembly of biomolecular condensates with shared components*, Phys. Rev. Lett. **126**, 258101 (2021).
[77] J. J. Hopfield, *Neurons with graded response have collective computational properties like those of two-state neurons.*, Proc. Natl. Acad. Sci. U.S.A. **81**, 3088 (1984).
[78] D. Bollé, T. M. Nieuwenhuizen, I. P. Castillo, and T. Verbeiren, *A spherical Hopfield model*, J. Phys. A **36**, 10269 (2003).
[79] A. V. Finkelstein and O. Ptitsyn, *Protein Physics: A Course of Lectures* (Elsevier, New York, 2016).
[80] J. A. Marsh and S. A. Teichmann, *Structure, dynamics, assembly, and evolution of protein complexes*, Annu. Rev. Biochem. **84**, 551 (2015).
[81] C. P. Brangwynne, C. R. Eckmann, D. S. Courson, A. Rybarska, C. Hoege, J. Gharakhani, F. Jülicher, and A. A. Hyman, *Germline p granules are liquid droplets that localize by controlled dissolution/condensation*, Science **324**, 1729 (2009).
[82] Thomas M. Fink and R. C. Ball, *How many conformations can a protein remember?*, Phys. Rev. Lett. **87**, 198103 (2001).
[83] P. Sartori and S. Leibler, *Lessons from equilibrium statistical physics regarding the assembly of protein complexes*, Proc. Natl. Acad. Sci. U.S.A. **117**, 114 (2020).
[84] H. Ramsauer, B. Schäfl, J. Lehner, P. Seidl, M. Widrich, T. Adler, L. Gruber, M. Holzleitner, M. Pavlović, G. K. Sandve *et al.*, *Hopfield networks is all you need*, arXiv: 2008.02217.
[85] A. Zentner, E. V. Halingstad, C. Chalk, M. P. Brenner, A. Murugan, E. Winfree, and K. Shrinivas, *Combinatorial decision-making driven by multicomponent surface condensates*, Proc. Natl. Acad. Sci. U.S.A. **123**, e2527873123 (2026).
[86] J. J. Hopfield, *Neurodynamics of mental exploration*, Proc. Natl. Acad. Sci. U.S.A. **107**, 1648 (2010).
[87] W. Zhong, D. J. Schwab, and A. Murugan, *Associative pattern recognition through macro-molecular self-assembly*, J. Stat. Phys. **167**, 806 (2017).
[88] M. L. Huggins, *Solutions of long chain compounds*, J. Chem. Phys. **9**, 440 (1941).
[89] S. R. De Groot and P. Mazur, *Non-Equilibrium Thermodynamics* (Courier Corporation, New York, 2013).